Tellus (1998), 50B, 263–289
Printed in UK – all rights reserved

TELLUS
ISSN 0280–6509

The impact of cloud particle gravitational settling on soluble trace gas distributions

By MARK G. LAWRENCE* and PAUL J. CRUTZEN *Max-Planck-Institut für Chemie, Abteilung Luftchemie, PF 3060, 55020 Mainz, Germany.*

(Manuscript recieved 13 October 1997; in final form 20 February 1998)

ABSTRACT

The effect of gravitational settling of cloud droplets and ice particles on the tropospheric distributions of soluble trace gases is examined, focusing in particular on nitric acid and hydrogen peroxide. For this study, we separate cloud condensate into two classes: large (rain, snow and graupel) and small (cloud water and cloud ice). The first class has typical fall speeds of several m/s and frequently reaches the ground. The redistribution and loss of soluble trace gases due to this type of precipitation is generally already included in global photochemical models (although the manner in which this is done varies widely between models). However, an additional redistribution can result from the gravitational settling of the second class, small cloud droplets or ice particles, whose mean fall speeds can reach 1 m/s. When we include this additional downward flux term in our model simulations, we find a significant impact on the distributions of the soluble trace gases HNO_3 and H_2O_2. In the upper troposphere, the settling of ice particles leads to a strong reduction in the mixing ratios of these gases, due to the relatively high terminal velocities of ice crystals (generally >10 cm/s). The impact of cloud droplet settling in the lower troposphere is also found to be significant in some regions, though it is generally smaller due to the slower settling velocities of liquid droplets; in addition, the settling loss in the lower troposphere is computed to be frequently overwhelmed by the supply of HNO_3 and H_2O_2 via sublimating hydrometeors settling in from above. Our findings may help explain the overestimate of free tropospheric HNO_3 found in several global photochemical modeling studies. The reductions computed for HNO_3 and H_2O_2 also have an effect on the distributions of related trace gases, such as NO_x and OH. Gravitational settling might also directly affect other soluble trace gases and aerosols. There are substantial uncertainties involved in computing the global impact of gravitational settling, such as the uptake of gases and aerosols onto and into ice particles and the high degree of variability and complexity of clouds. Results of sensitivity studies examining some of these uncertainties are presented. Even employing a low-end settling velocity for ice particles (5 cm/s) and a minimum ice uptake efficiency for HNO_3 based on laboratory data, we still compute a notable impact on the upper tropospheric HNO_3 and H_2O_2 distributions.

1. Introduction

Clouds are of critical importance to atmospheric chemistry due to their role in convective transport, precipitation scavenging, radiative transfer (which determines photolysis rates), and as media for photochemical reactions occurring in and on cloud droplets and ice particles. The sub-gridscale processes associated with clouds are difficult to parameterize in global models. An example of this is convective transport, which generally occurs on horizontal scales of about ten kilometers, which is much smaller than the typical global model grid

* Corresponding author.

cell dimension of 100 km or greater. Another example is non-convective vertical motion of air. In global models, this is generally approximated as a single upward or downward velocity over an entire grid cell, whereas in reality, especially in the presence of cloud fields, vertical motions will more commonly be present as a "patchwork" of much faster updrafts and downdrafts, the (much smaller) difference of which is represented by the residual vertical motions considered in global models. In addition to only being able to approximate the effects of these sub-gridscale processes, there are some processes whose effects are at present left out entirely.

One process of potential importance which has thus far been generally neglected in global tropospheric photochemistry models (GTPMs) is the gravitational settling and subsequent evaporation of cloud droplets and ice particles, which imparts an effective downward velocity to soluble trace gases and aerosols. The process we will refer to as "gravitational settling" is the downward sedimentation of "small" cloud particles, where "small" means any cloud particles that would not be commonly considered to be rain, snow, or graupel (which we will call "precipitate"). The mean downward velocities of these small cloud particles are usually $\leqslant 1$ m/s, much slower than the fall speeds of precipitate. For this reason, the settling of small particles before they evaporate has generally been disregarded in GTPMs. However, only a small fraction (order 10%) of clouds are predicted to produce precipitate before they dissipate. Integrated over time, the slower motion of the remaining cloud water/ice could potentially influence tropospheric chemistry by redistributing soluble trace gases contained in the particles to lower levels. In the present study, we show that gravitational settling is likely responsible for a significant loss of HNO_3 and H_2O_2 from the upper troposphere. The same may apply to other soluble gases and aerosols. The neglect of this process may explain why several GTPMs have been found to substantially overestimate upper tropospheric HNO_3 compared to available observations (Lawrence, 1996; Wang et al., 1998; J.-F. Mueller, personal communication, 1997).

The gravitational settling mechanism we are considering here is not the same as the process that is commonly referred to as "wet deposition" (or "precipitation scavenging"), though it is similar in nature. Precipitation scavenging is the redistribution and removal of soluble trace gases by precipitate (i.e., rain, snow, and graupel). Precipitate particles have fall speeds of several m/s, and commonly reach the ground. When they do fall to the surface, then any soluble trace gases they contain are lost from the atmosphere. If they instead evaporate before reaching the surface, then their trace gas contents are released back to the gas phase (or kept in the aerosol phase), but redistributed to lower altitudes. A representation of the loss of trace gases to precipitation scavenging is generally incorporated into GTPMs, though in a variety of ways. Some models employ simple regional climatological loss frequency coefficients based on observed rainfall amounts. Others (including the model used in this study) employ complex algorithms that follow precipitate (and trace gases residing in the precipitate) as it percolates down through model levels, based on model-computed precipitate formation and evaporation rates at each level. In either case, the focus has been on the redistribution and loss due to rapidly-falling precipitate, generally not accounting for the slower-moving cloud water and ice particles.

Consideration of the possible role of gravitational settling in determining tropospheric trace gas distributions dates back to Crutzen and Gidel (1983), who incorporated a simple treatment of the settling of water vapor and water-soluble gases into a two-dimensional model. However, the mean settling velocities arrived at based on their assumptions were considerably slower than those employed here, especially for ice particles. Since then, little attention has been given to this process in GTPM simulations. In contrast, for stratospheric chemistry, gravitational settling has been recognized as an important process leading to denitrification and dehydration of the polar stratosphere (Fahey et al., 1990). In addition, the impact of gravitational sedimentation on tropospheric climate simulations due to its influence on water vapor and precipitable water distributions has been shown to be significant (e.g., Mitchell et al., 1989).

The settling mechanism which we are attempting to simulate for the global troposphere is actually a highly complex process on a cloud scale, and will vary considerably from cloud to cloud. In some clouds, e.g., detached cirrus, some intermediate-sized particles which form in the

cloud will sediment out of the base of the cloud and fall considerable distances (up to a few kilometers) before sublimating (Heymsfield and Donner, 1990; Hall and Pruppacher, 1976), yet these same particles would not be considered as precipitation in many GTPMs. In other clouds, e.g., stable marine stratiform which extend over several model grid cells, the mean settling velocity of the cloud droplets roughly balances the large scale upwelling motion through the clouds, so that the clouds on the whole remain at a fairly constant altitude. In the air that is transported through these stable cloud layers, soluble and non-soluble trace gases will be physically separated from each other. However, large-scale transport (advection) routines in global models are generally not made aware of the degree of solubility of trace gases or the presence of clouds. In still other instances, sub-gridscale clouds might form with particles that are large enough that they sediment at an average rate faster than the ascension rate of air through the clouds, leading to a sedimentation of the entire cloud over time; this is also generally not accounted for in GTPMs.

Our objective is to determine whether or not the global effect of this mechanism is potentially significant enough that it should be generally incorporated into GTPMs. For the sake of global simulations, it is at present necessary to considerably simplify the picture of the settling mechanism given in the preceding paragraph. In doing so, we employ semi-empirical relationships in order to derive an estimate of the mean settling motion on a scale appropriate to a global model, and based on parameters currently available in the model (e.g., cloud water/ice content). In the following sections, we first describe the global model framework in which we conduct this study, focusing on the cloud processes which are relevant to this mechanism. Then we describe the derivation of mean settling velocities for use in the model simulations. Following this, we present the results of several sensitivity studies which examine the global impact of this mechanism, and we conclude with a discussion of uncertainties and recommended future studies.

2. Approach

2.1. Model description

We employ the Max-Planck-Institute for Chemistry version of the model MATCH (Model of Atmospheric Transport and CHemistry), which is described and evaluated elsewhere (Rasch et al., 1997; Mahowald, 1996; Mahowald et al., 1997 (a,b); Lawrence, 1996). In brief, MATCH is a global offline tracer model. The simulations here are driven by meteorological data from the National Centers for Environmental Prediction (NCEP) reanalysis (Kalnay et al., 1996) which has been reduced to a T21 grid (about 5.6×5.6 degrees in the horizontal), with 28 vertical sigma levels between the surface and about 2 hPa. The reduced resolution horizontal grid gives results for the photochemical simulations similar to the high resolution grid, but allows sensitivity studies to be more readily conducted. The vertical structure of the layers is given in Table 1. The layers are closely spaced near the surface, and become less resolved in the free troposphere, where the typical layer thickness is order 50–65 hPa, or about 1–2 km.

The convection parameterization employed in this version of MATCH is the same as that used in the NCEP model (Pan and Wu, 1995). The Pan-Wu scheme provides convective mass fluxes (updrafts and downdrafts) for trace gas redistribution, as well as convective precipitation formation and evaporation rates. The parameterization is essentially a simplified Arakawa-Schubert scheme (Arakawa and Schubert, 1974). The implementation in MATCH (Mahowald, 1996) allows entrainment only at the cloud base, and detrainment only at the top layer of the convective cloud, with no mixing along the column. For this study, the implemented version has been modified to prevent excessive convective transport of soluble trace gases. This is done by allowing only the interstitial phase of soluble trace gases to be acted upon by the convective core updrafts and downdrafts. For a highly soluble trace gas such as HNO_3, this results in negligible upward transport by deep convective core updrafts, since virtually none of the HNO_3 will be in the gas phase; for a semi-soluble gas such as H_2O_2, this can also result in a significant reduction of upward transport compared to that of non-soluble gases (e.g., NO_x). This could result in an underestimate of the vertical transport of these trace gases, because it does not account for the possible source due to cloud particles which originate in lower layers and are ejected into the upper troposphere, releasing their trace gas contents upon sublimation; such details of convective transport require further study. It is

Table 1. *Sigma levels for the MATCH simulations in this study*

Level	Upper boundary	Midpoint	Lower boundary	Layer thickness
1	0.001	0.003	0.007	0.006
2	0.007	0.010	0.014	0.007
3	0.014	0.018	0.023	0.009
4	0.023	0.029	0.035	0.012
5	0.035	0.042	0.049	0.014
6	0.049	0.058	0.067	0.018
7	0.067	0.078	0.089	0.022
8	0.089	0.103	0.116	0.027
9	0.116	0.133	0.149	0.033
10	0.149	0.168	0.188	0.039
11	0.188	0.210	0.233	0.045
12	0.233	0.258	0.284	0.051
13	0.284	0.313	0.341	0.057
14	0.341	0.372	0.403	0.062
15	0.403	0.436	0.469	0.066
16	0.469	0.502	0.535	0.066
17	0.535	0.568	0.601	0.066
18	0.601	0.633	0.665	0.064
19	0.665	0.694	0.724	0.059
20	0.724	0.751	0.778	0.054
21	0.778	0.801	0.825	0.047
22	0.825	0.846	0.866	0.041
23	0.866	0.884	0.901	0.035
24	0.901	0.916	0.930	0.029
25	0.930	0.942	0.955	0.025
26	0.955	0.964	0.974	0.019
27	0.974	0.982	0.990	0.016
28	0.990	0.995	1.000	0.010

The sigma values given in the table times the surface pressure give the pressure for that particular level or interface, $P = \sigma P_s$; e.g., for a surface pressure of 900 hPa, the upper boundary of layer 10 would be 134.1 hPa (= 0.149*900). Note that MATCH actually uses a hybrid coordinate η, but for the NCEP data the hybrid coordinate is identical to a sigma coordinate ($\eta = \sigma$).

important to note that we do not apply our gravitational settling algorithm (described below) to the cloud water in the cores of convective clouds. In this study we are only considering the settling motion of cloud water/ice in "large-scale" clouds, such as stratiform, fair weather cumulus, and cirrus (both attached anvils and detached).

A critical parameter for our study is the cloud water/ice content, i.e., the small (non-precipitate) particles which are subject to the gravitational settling described above. This is provided by the cloud microphysics parameterization in MATCH (Rasch and Kristjansson, 1998). The scheme, which will become part of the next generation of the NCAR Community Climate Model 3 (CCM3), actually considers four different types of cloud condensate: two forms of suspended condensate (cloud water and cloud ice), and two forms of precipitate (rain and snow/graupel). However, the only term which is stored and integrated over time is the total suspended condensate, cloud water + cloud ice; the other terms are derived from this value and ambient conditions each time step, as described below.

The partitioning between cloud water and ice is treated as a simple function of the temperature, linearly interpolated between 100% water at 0°C (and above) and 100% ice at −20°C (and below). The rates of condensation and evaporation of water vapor onto and from cloud water/ice are based on the formulation of Sundqvist (1978, 1993), which primarily depends on the relative humidity and the rate of moistening or drying of a grid cell over a time step. The conversion from suspended condensate (cloud water/ice) to precipitate (rain and snow/graupel) occurs due to several processes: conversion (growth) of cloud water to rain, collection of cloud water by falling rain, auto-conversion of cloud ice to snow, and collection of cloud water and ice by falling snow. Each of these terms is computed individually based on the cloud water/ice mixing ratio, conversion rate coefficients and thresholds, and ambient parameters (e.g., air density). The sum of these terms gives the loss of suspended cloud water/ice during a time step, and the formation rate of the precipitate phase which falls out of the cell. Finally, evaporation of precipitate falling through cloud-free regions is also allowed, based on the ambient relative humidity, following Sundqvist et al. (1989). The end result of these computations is the provision of three-dimensional time-dependent cloud water and ice contents resembling those observed in several studies (McFarquhar and Heymsfield, 1997; Gultepe and Isaac, 1997; Mazin, 1995), as well as also providing large-scale (non-convective) precipitation fluxes. It is worth noting that in Rasch and Kristjansson (1998), the simulated cloud ice amounts tended to be somewhat low compared to in situ observations. This is done intentionally in the CCM3 to keep from overestimating reflected solar radiation fluxes, since clouds with ice water contents as high as typically observed in situ are generally computed by the

CCM3 to be too bright compared to satellite observations (P. Rasch, pers. comm., 1997). For these simulations with MATCH, we have obtained cloud ice amounts which agree better with in situ observations by adjusting the autoconversion threshold for cold ice to a higher value (so that higher ice contents can exist prior to the onset of precipitation).

The critical point to understand about the present form of the parameterization is that the cloud water and cloud ice are assumed to be "suspended condensate with no appreciable fall speed" (Rasch and Kristjansson, 1998). It is the sensitivity of tropospheric trace gas distributions to this assumption that we are considering here. Below we will determine first what kinds of fall speeds are typical for the "suspended" (cloud water/ice) part of the condensate, and then apply this towards redistributing the soluble trace gases HNO_3 and H_2O_2. One should realize that not all cloud microphysics schemes make the assumption that a separate suspended cloud water/ice partition exists; Roeckner et al. (1996), for instance, instead take the simpler approach of grouping all the ice condensate into one bulk phase, and then apply sedimentation (precipitation) to the entire bulk ice amount. However, we are not aware of any GTPMs that have yet taken into account the sedimentation of the entire spectrum of liquid and ice particles for determining soluble trace gas distributions.

The nitric acid and hydrogen peroxide simulations considered here are part of the basic tropospheric chemistry module developed for use in MATCH (Lawrence, 1996), which includes emissions of NO_x, CO, and CH_4, photochemical transformations within the O_3-HO_x-NO_y-CH_4-CO framework, and losses due to oxidation and wet and dry deposition. The distributions of key trace gases (O_3, CO, and NO_x) computed by MATCH generally compare well to observations, with the notable exception of a persistent substantial overestimate of free tropospheric HNO_3 amounts (Lawrence, 1996).

In addition to the redistribution due to gravitational settling of smaller cloud water/ice particles, which we are examining in this study, the larger precipitate particles (rain, snow, and graupel) are also important in determining trace gas distributions. In MATCH, we already account for the precipitation scavenging ("wet deposition") by these larger precipitate particles. To determine wet deposition losses, we use the time-dependent information on precipitate formation available from the convection and cloud microphysics components of the model.

For each soluble trace gas (e.g., HNO_3, H_2O_2), we determine the amount which is lost from each grid cell due to formation of new precipitate ("rainout") by multiplying the flux of precipitate out of a layer times the condensed phase concentration of the soluble gas in the precipitate. We similarly compute the amount of each soluble trace gas which will be scavenged from each layer by precipitate which formed at higher altitudes and falls through the layer ("washout"). Finally, if any of the precipitate evaporates below the cloud base, it can (depending on the solubility of the gas in question and the degree of evaporation) release some or all of the trace gas back into the environment. These three terms together (rainout loss + washout loss + evaporative source) determine the change in the soluble trace gas concentration in each layer during a time step due to precipitation scavenging.

Our base case simulation (see below) considers only this type of scavenging, that is, the redistribution due to only the precipitate part of the cloud condensate. This can be considered as a standard case for current GTPMs. We then include the additional redistribution of HNO_3 and H_2O_2 due to the gravitational settling of the smaller cloud water/ice particles. It will be seen that accounting for this additional settling motion can have a significant effect on the distributions of soluble trace gases.

2.2. *Ice particle and liquid droplet terminal velocities*

In order to compute the effect of gravitational settling on HNO_3 and H_2O_2, we must first determine settling velocities for cloud water/ice (i.e., for the non-precipitate part of the cloud condensate). We do this by examining typical fall velocities of particles in clouds which are not producing precipitate. In considering these velocities, it is important to realize that a detailed simulation of the settling process requires parameters that are not yet available in our global simulations, such as cloud particle size and shape distributions. Our focus is thus on using fall velocities which are representat-

ive of the mean settling motion for clouds in the context of the moderately low horizontal resolution of a global model. Settling velocities strongly depend on cloud type. The most important difference is between liquid and ice clouds; ice particles tend to have much higher terminal velocities due to their larger size. We account for this difference by employing different parameterizations for liquid ($T > 0°C$) and ice ($T \leqslant -20°C$) clouds. We assume a linear transition from liquid to ice clouds for temperatures between 0°C and −20°C.

For ice crystals, we split the characteristic terminal velocities used in our simulations into two latitude regimes, summarized as:

$$V_t = \begin{cases} \min(100,\ 128.6 + 53.2\ \log_{10}(\mathrm{IWC}) \\ \qquad +5.5\ [\log_{10}(\mathrm{IWC})]^2), & |\mathrm{lat}| \leqslant 30^\circ \\ \min(100,\ 109(\mathrm{IWC})^{0.16}), & |\mathrm{lat}| > 30^\circ \end{cases} \quad (1)$$

where V_t is the mass-weighted ensemble mean fall velocity (cm/s), and IWC is the ice water content in g/m^3. The IWC values for use in the equation are taken from the microphysical parameterization in MATCH (Rasch and Kristjansson, 1998). For the tropical band, the parameterization for V_t is derived based on measurements of ice cloud properties (e.g., ice water content, crystal shape and dimensions) made during the Central Equatorial Pacific Experiment (CEPEX), in which several detached cirrus anvils between 7 and 14 km were probed for properties such as ice water content, characteristic crystal shape, and mean crystal dimensions, employing optical array probes located on board a Learjet (McFarquhar and Heymsfield, 1996; Heymsfield and McFarquhar, 1996). These properties were then used to compute V_t for each 10-s (2 km) average of data taken on the Learjet. Depending on the size and shape of the crystal and ambient conditions (e.g., air density), the terminal velocity was calculated following the equations outlined in Heymsfield (1972), Heymsfield and Kajikawa (1987), and the references contained therein. The mass-weighted terminal velocity was then calculated by integrating the individual crystal terminal velocities over all observed crystal sizes and shapes. It was found that the best first-order relationship for the data exists between V_t and the ice water content (G. McFarquhar and A. Heymsfield, pers. comm. 1997); the fit to this relationship is used in our simulations for the tropics (see eq. (1)). Similarly, for extratropical latitudes the mean terminal velocity is based on the parameterization in Heymsfield and Donner (1990), which is in turn based on cirrus cloud observations over North America made by Heymsfield (1977), combined with computations similar to those described above for the CEPEX data.

These two parameterizations give terminal velocities that typically range from about 5 to 100 cm/s. For example, for a low-end ice water content of 0.0001 g/m^3, V_t is computed to be 4 cm/s for the tropics and 25 cm/s for the extratropics. For a typical high-end IWC of 0.1 g/m^3, V_t is 81 cm/s and 75 cm/s for the tropics and extratropics, respectively. We have chosen to limit the maximum V_t employed in our simulations to 100 cm/s, although larger mean settling velocities would be possible for clouds with high ice water contents. Given the uncertainty in computing mass-weighted ensemble mean terminal velocities, and particularly in extrapolating them to values for use on a large-scale basis, we also perform sensitivity simulations using a constant low-end value for V_t (5 cm/s), above which most computed and measured mean V_t values for cloud ice particles lie.

For liquid clouds, we assume Stokes flow, that is, $V_t(r_d) = k_s r_d^2$ for a single droplet, where k_s is the Stokes constant (1.19×10^6 cm^{-1} s^{-1}) and r_d is the droplet radius. In order to determine the ensemble mean settling velocity for the wide range of droplet sizes found in a cloud, we assume a Khrgian-Mazin (gamma) distribution for the cloud droplets (Pruppacher and Klett, 1997), and compute the mass-weighted integral of the Stokes velocity across this distribution. This yields $V_t = 4.67\ k_s r_m^2 = 1.68\ k_s\ r_e^2$, where r_m is the arithmetic mean radius, and r_e is the effective radius (the third moment of the radius weighted by the second moment). The effective radius is related to the mean radius by $r_e = 1.67\ r_m$ (for the Khrgian-Mazin distribution). We can also similarly define an effective settling radius, r_s, for which the Stokes equation holds: $V_t = k_s r_s^2$, where $r_s = 2.16\ r_m$. This shows the importance of the square dependence of fall velocity on droplet radius, since the effective radius for settling is over twice as large as the arithmetic mean radius.

Data on the mean effective radius in clouds on

a global scale is available from the AVHRR satellite study of Han et al. (1994), who find r_e to be 8.5 μm over land and 11.8 μm over ocean. These are equivalent to arithmetic mean radii (r_m) of 5.1 μm and 7 μm, respectively, and to effective settling radii (r_s) of 11.0 μm and 15.3 μm, respectively. Using these radii, the mass-weighted ensemble settling velocity (V_t) is computed to be 1.5 cm/s over land and 2.8 cm/s over ocean. We use these as our standard values for the settling velocities of liquid cloud droplets. There are two reasons, however, why these settling velocities might be underestimates.

First, it has been found that satellite-based measurements tend to underestimate cloud droplet radii compared to in situ observations. The in situ observations compiled in Heymsfield (1993) indicate mean radii (r_m) of about 6.5 μm over land and 9.7 μm over ocean, which convert to effective radii (r_e) of about 10.8 μm and 16.2 μm, respectively (and $r_s = 14$ and 21 μm, respectively). These would imply terminal velocities up to 2 times as high as those based on the satellite-derived effective radii. The exact reason for the discrepancy between satellite and in situ observations is not yet known. A possible explanation is that satellite radiometers become saturated (and hence insensitive) for optical thicknesses greater than about 3, and thus will be biased towards representing the upper regions of liquid water clouds (A. Heymsfield, personal communication, 1997). Although cloud droplet radii do not always decrease with height (the opposite is true for average stratiform clouds), they may do so often enough to allow this bias to be the cause of the discrepancy. Another possibility is that the degree of sampling by in situ measurements is still too sparse to adequately represent "average" clouds on a global scale; whether this is the case will become clearer in ongoing field campaigns. Since there is no strong evidence as yet supporting either set of radii over the other, we have chosen to use the smaller radii (satellite values) as our standard values and the larger in sensitivity simulations.

A second reason our base velocities might be underestimates is that highly soluble species such as HNO_3 will be predominantly taken up in the droplets which form first, which will also tend to grow to larger sizes and fall more quickly than the ensemble mean. It is, however, difficult to quantitatively estimate the effect this partitioning might have on fall velocities. We have thus chosen to also conduct a simulation in which we employ liquid water terminal velocities which are four times those based on the satellite-derived radii (i.e., 6 cm/s over land, and 11.2 cm/s over ocean), in order to examine the sensitivity of the results to the liquid droplet settling velocities which are assumed.

2.3. *Determining effective (grid cell mean) settling velocities*

The cloud particle terminal velocities described above then need to be applied to modify the simulated HNO_3 and H_2O_2 tracer fields. This is done by first computing an effective settling velocity, V_e, which is a mean velocity used to calculate the flux across the lower face of a cell volume (i.e., the velocity which acts on the trace gas averages across the entire grid cell). This effective velocity is then passed into a 1D advection algorithm (P. J. Rasch, personal communication, 1997), which computes vertical HNO_3 fluxes based on V_e and the HNO_3 vertical profile. This advection scheme is employed in order to reduce numerical diffusion problems, which we have found can occur when simpler approximations (e.g., Euler forward) are used for computing the HNO_3 flux. For any soluble gas, the effective velocity to use in the vertical advection scheme is computed as:

$$V_e = V_t F_{cld} F_p \tag{2}$$

where V_t is the mean terminal velocity as discussed above, F_{cld} is the cloudy fraction of the grid cell, and F_p is the fraction of the tracer which is in the cloud particles (in the cloudy part of the cell).

F_{cld} in MATCH is based on the scheme of Slingo (1987), which determines the cloudy fraction primarily as a function of relative humidity (as well as a function of latitude and vertical velocity). This gives the zonal mean global cloud cover distribution for July depicted in Fig. 1, which is in basic agreement with cloud atlases (Warren et al., 1986; Lelieveld et al., 1989). In our simulations, we take F_{cld} to indicate the fractional volume of each grid cell which is occupied by cloud. Although for a typical global model grid cell size the clouds will frequently be spread out as a "patchwork" throughout the cell, both in the horizontal and vertical dimensions, we are currently not capable of treating this kind of sub-

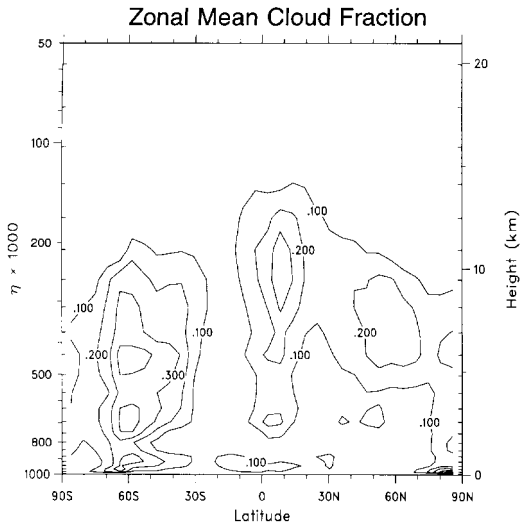

Fig. 1. The zonal mean cloud fraction distribution for our July, 1993 MATCH simulation. For this and all other latitude-height contour plots, the scale at the left is the hybrid coordinate η (see Table 1 footnote) times 1000, which gives the approximate pressure in hPa. The model layer interfaces are indicated on the figure by inward-pointing tickmarks. An approximate altitude scale is also given on the right.

gridscale detail. We will assume that the clouds in a given gridcell always extend from the bottom to the top of the level over the fraction F_{cld} in the horizontal, so that we can formulate the effective settling velocity for the cell as in eq. (2). This is consistent with the assumptions about the subgridcell cloud distribution in other model parameterizations (e.g., precipitation scavenging, radiative transfer).

The value of F_p depends either on the solubility of the tracer in liquid water, or on how efficiently the tracer is taken up onto and into ice particles. For HNO_3, $F_p \approx 1$ for liquid clouds, due to its extremely high solubility. For ice clouds, it is not yet completely clear how efficient the uptake of HNO_3 is. Two recent studies indicate an uptake of at least $1–3 \times 10^{14}$ molec/cm^2 on ice particle surfaces (Abbatt, 1997; Zondlo et al., 1997). Abbatt (1997) also indicates that this process appears to be largely irreversible. If HNO_3 is readily incorporated into the ice particles as they grow, then F_p will be nearly one. Unfortunately, there is as yet no experimental data investigating incorporation of HNO_3 into the bulk phase. However, there is reason to suspect that this may occur for HNO_3 based on experiments which demonstrate that under stratospheric conditions HNO_3 is extremely readily incorporated as NAT (nitric acid trihydrate) into the ice bulk phase (U. M. Biermann, personal communication, 1997). Nitric acid might behave similarly, even though NAT is not formed under tropospheric conditions. In the stratosphere, NAT is frozen directly into the ice crystal matrix immediately upon its formation. On the other hand, HNO_3 in the troposphere can form a quasi-layer on the ice surface. Unless new water vapor passes through the HNO_3 quasi-layer and freezes below, leaving the HNO_3 still sitting on the surface, HNO_3 will freeze along with the H_2O and be trapped into the ice particle. We will assume that $F_p = 1$ for HNO_3 in both liquid and ice phases; however, in addition, we perform a sensitivity run (LOWUPTAKE, see Table 3) in which we limit the uptake on ice to only 10^{14} molec/cm^2.

For the limited-uptake simulation, we also need to know the amount of surface area available on ice particles in a cloud. This could be estimated from the model ice water contents by simply assuming a particle number density and shape and size distribution, though the error inherent in such rough assumptions would be large. We have instead decided to employ an empirical relationship given in Heymsfield and McFarquhar (1996) based on observations made during CEPEX, which relates the cross-sectional area of particles in an ice cloud to the IWC:

$$A_c = 10^{-4} \mathrm{IWC}^{0.9} \tag{3}$$

giving the cross sectional area A_c in cm^2/cm^3 when IWC is in g/m^3. For example, for an IWC of 0.1 g/m^3, eq. (3) would give $A_c = 1.3 \times 10^{-5}$ cm^2/cm^3, while for a low-end IWC of 0.0001 g/m^3, A_c would be 2.5×10^{-8} cm^2/cm^3. The parameter we are actually interested in, however, is A_s, the surface area density, rather than A_c. The relationship between A_s and A_c depends on the shape of the ice crystals. For instance, for a spherical particle with radius r_i, the surface area is $A_s = 4\pi r_i^2$, while the cross-sectional area is $A_c = \pi r_i^2$, yielding $A_s = 4A_c$. For cubes, depending on the orientation of the cube being projected onto a 2D plane, the ratio of A_s/A_c varies from 3–6. The minimum ratio possible for A_s/A_c is just over 2, occurring for flat plates and dendrites seen from the planar view. If we assume $A_s = 2A_c$, then

the minimum amount of HNO_3 which should be taken up onto the ice crystals can be estimated (assuming coverage of 10^{14} molec/cm^2). For example, for an IWC of 0.01 g/m^3, the surface area density is computed to be $A_s = 3.2 \times 10^{-6}$ cm^2/cm^3, implying a minimum uptake of 3.2×10^8 molec/cm^3, which converts to about 40 ppt for the upper troposphere. This is in the range of typical tropospheric HNO_3 levels, indicating that this limitation could be of importance. The degree of importance will be assessed by including this limitation in a sensitivity simulation. We do this for each cloudy grid cell by computing the minimum amount of HNO_3 which should reside on the ice particle surfaces as described above. Let us call this amount $[HNO_3]_{ice}$, and call the concentration of total HNO_3 (interstitial plus condensed) in the cloudy part of the grid cell $[HNO_3]_t$. We can then compute the ratio $F_p = [HNO_3]_{ice}/[HNO_3]_t$. This is the same F_p as in equation (2), which is applied in the sensitivity run to obtain appropriately modified V_t values, so that settling is only being allowed to act on the HNO_3 which would reside on the ice particle surfaces (according to Abbat, 1997, and Zondlo et al., 1997).

In addition to the laboratory evidence of the uptake of HNO_3 on cirrus ice, there is now also in situ evidence that this occurs. Weinheimer et al. (1998) examined the difference between NO_y measurements in the forward and aft intakes on an aircraft flying through wave cirrus over Colorado. The two intakes differ in how they capture ice particles (the aft intake being biased against ice particles). In the clouds, they found an amount of condensed-phase NO_y corresponding to 10–20% of the gas-phase amount, presumably due to uptake of HNO_3 on the ice particles. Using the model of Jensen et al. (1998), they also computed that one would expect complete uptake of HNO_3 to be possible within 1–2 min, so that gas phase diffusion would not present a limitation to HNO_3 uptake (note that we would thus generally expect gas phase diffusion not to be a limitation, since the ice water content used in the calculations of Weinheimer et al. was $3–6 \times 10^{-3}$ g/m^3, which is at the low end of ice water contents in clouds that are important for gravitational settling). Weinheimer et al. interpret their observations as indicating that it is likely that they were observing complete uptake of HNO_3, i.e., that the HNO_3/NO_y ratio where they were sampling was about 0.1–0.2. Although they noted that this is considerably lower than the typical ratio of HNO_3/NO_y computed by models for this region (30–50%), they find it consistent with observations in other regions (e.g., the western Pacific and south Atlantic). We propose that the discrepancy with other models is perhaps due to the neglect of small particle gravitational settling in these models, which we will show below considerably reduces the amount of simulated HNO_3 in the upper troposphere.

For H_2O_2, the solubility in liquid water is less than that for HNO_3; we compute F_p for each liquid water cloud based on the Henry's Law coefficient for H_2O_2 (Lind and Kok, 1986). For ice, we use data from the study of Conklin et al. (1993a). Their experiments, aimed at understanding uptake of H_2O_2 on surface snow at the poles, indicated that H_2O_2 is reversibly incorporated into the bulk phase of ice, and that the partitioning between gas and condensed phase is strongly temperature dependent, being higher for lower temperatures. Their data for partitioning of gas and condensed phase H_2O_2 at four temperatures is listed in Table 2. The value of K_D gives the ratio of the H_2O_2 density in the ice (molec/cm^3_i) to the density in air (molec/cm^3_a). Multiplying this value by a cloud ice volume mixing ratio, IWC_v (cm^3_i/cm^3_a), then gives a dimensionless fraction of the amount of H_2O_2 in the ice versus in the air. Since the total H_2O_2 in a grid cell will be partitioned into the condensed and gas phases, the fraction of total H_2O_2 which is in the ice can be

Table 2. *Uptake partitioning constant K_D for H_2O_2 in ice as a function of temperature*

T (°C)	K_D *(expt)* (cm^3_a/cm^3_i)	K_D (fit) (cm^3_a/cm^3_i)
−3	8.30×10^4	8.79×10^4
−11	1.24×10^5	1.19×10^5
−30	5.78×10^5	5.47×10^5
−45	1.07×10^7	1.05×10^7

The experimental data, K_D (expt), is from Conklin et al. (1993a). The fit to the data, K_D (the form K_D (fit), is of the form $K_D = a^* \exp(b10^{(-T/c)})$, where T is the temperature (degrees C), and the optimal (least squares fit) coefficients are $a = 5 \times 10^4$, $b = 0.48$, and $c = 43$.

computed as $F_p = K_D\ \mathrm{IWC_v}/(1 + K_D\ \mathrm{IWC_v})$. In order to use the Conklin et al. (1993a) data to compute F_p for our simulations, we need to fit a smooth curve to the data. The curve we have chosen for this purpose has the form $K_D = a \exp(b\ 10^{(-T/c)})$, where T is the temperature (degrees C). Optimal values for the coefficients, $a = 5 \times 10^4$, $b = 0.48$, and $c = 43$, were found by searching the parameter space for the set of coefficients that provided the least squares fit to the data at the four available temperatures. The quality of the fit can be seen in Table 2, where the fit values for K_D are also listed; they are generally within about 5% of the observations. It is worth noting the possibility that these data underestimate the uptake which will occur in clouds, since the measurements of Conklin et al. (1993a) were made with a stable snow layer in mind; cloud ice particles, on the other hand, will often be growing over time, which might enhance the trapping of H_2O_2 into the bulk phase. To see the potential implications of this, we conduct an additional run in which we set $F_p = 1.0$ for H_2O_2.

It is thus possible to compute mean effective settling velocities for HNO_3 based on eq. (2), and to compare these to advective and convective redistribution mean velocities. This is done in Fig. 2, which shows that for HNO_3, V_e is larger than the mean advective and convective velocities throughout most of the troposphere (note that the upward and downward components of advection are shown individually, and the convective velocities shown are only the core updraft component, averaged over each grid cell). For H_2O_2, the computed effective settling velocities (not shown) are somewhat slower due to its less efficient uptake into liquid and ice cloud droplets; however, in some regions (especially the upper troposphere) they are still faster than the other atmospheric motions shown here. These high zonal mean effective settling velocities would lead one to expect a significant impact on tropospheric HNO_3 and H_2O_2 in the simulations, which is indeed seen in the results of several simulations.

2.4. *Model simulations description*

Several cases are considered here, outlined in Table 3. The BASE run is without the effect of gravitational settling (but with the standard precipitation scavenging as described earlier). STDFALL differs from the BASE simulation in that it includes gravitational settling for all non-convective-core cloud water/ice, with the following "standard" assumptions: ice particle settling velocities as outlined in equation (1); liquid droplet settling velocities computed from the satellite-based radii as described earlier; and ice particle uptake efficiencies of 100% for HNO_3, and based on Table 2 for H_2O_2. The case STDVI + 4VL (only for HNO_3) examines the possible effects of $4\times$ faster liquid settling velocities than in the STDFALL run (but keeping the standard fall velocities for ice). HIUPTAKE (only for H_2O_2) examines the implications of a possible 100% uptake efficiency for H_2O_2 on ice particles. The SLOWICE and LOWUPTAKE runs consider the sensitivity to ice particle settling alone (i.e., no liquid settling), using $V_t = 5$ cm/s for ice, which is at the low end of what is generally indicated by most studies of ice crystal terminal velocities. LOWUPTAKE (only for HNO_3) differs from SLOWICE in that the uptake of HNO_3 onto ice particles is limited to 10^{14} molec/cm^2. The final two cases, STDLIQ and FASTLIQ, consider the impact from settling of liquid cloud drops alone (i.e., no ice settling), with FASTLIQ employing liquid settling velocities which are four times as fast as the velocities used in STDLIQ.

The simulations start in June (1993) and allow a one-month spinup before results are considered. The model is initialized with mean tracer distributions for June from a longer run (without the settling effect). We have chosen a time step, Δt, of 15 min to limit numerical problems. This time step is small enough that generally $V_e \Delta t/\Delta z < 1$, where Δz is the model layer thickness (typically 1–2 km in the free troposphere). In some instances near the surface at high latitudes (where the layers are thinner and ice clouds can form in the lower troposphere), this condition can be exceeded; in that case, the flux out the bottom of each cell is limited to at most being able to remove the amount of tracer available in the cloudy part of the cell.

In the simulations, we assume that at the end of each time step, all of the HNO_3 and H_2O_2 contained in the particulate phase which falls into the cell below then evaporates back into the gas phase for the sake of the photochemistry and the other transport algorithms. It is certainly possible that some cloud particles would fall through more

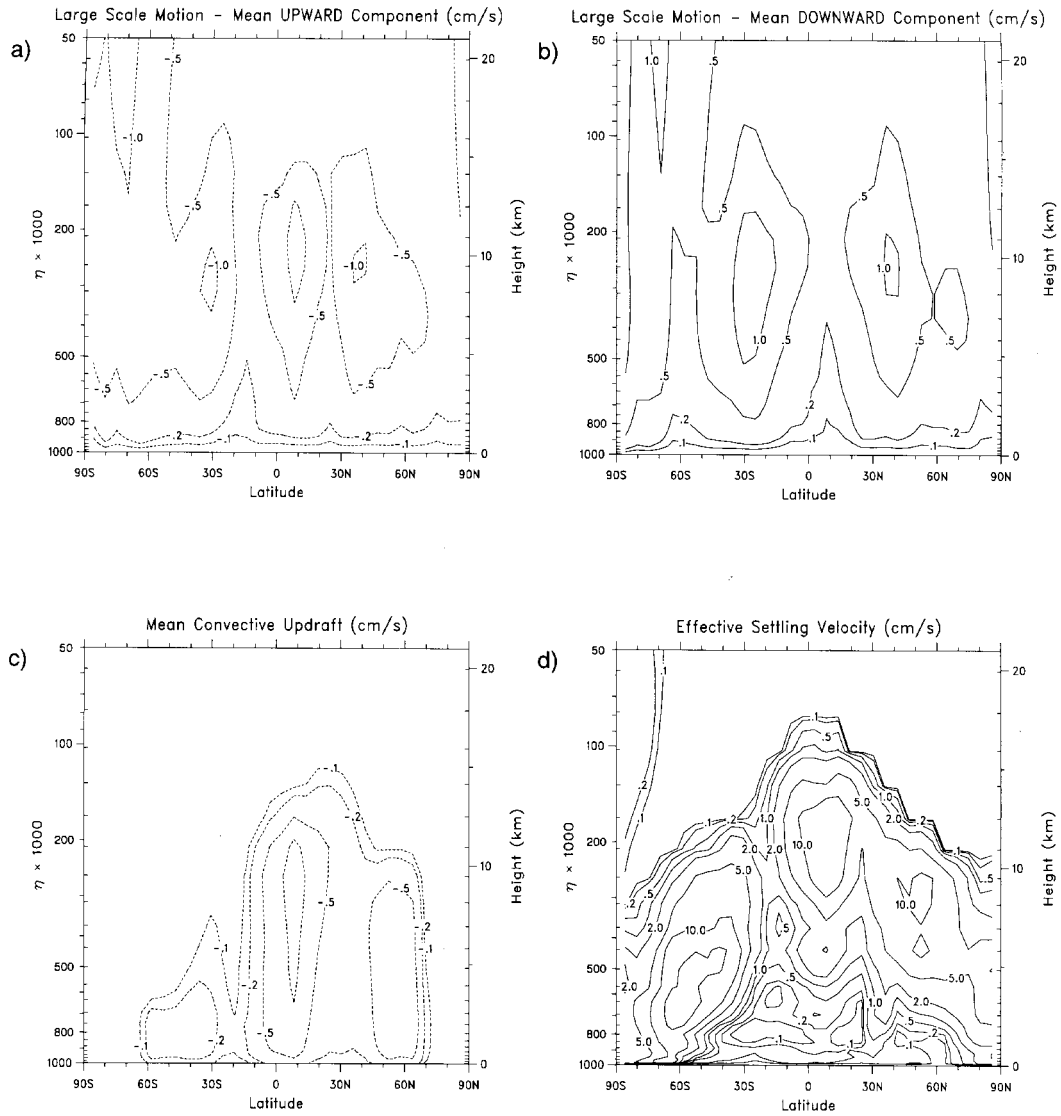

Fig. 2. Zonal mean transport velocities (solid lines are downwards and dotted lines are upwards), all means for July, 1993, of the simulation: (a) upwards component of advective (large scale) motion, (b) downwards component of advective (large scale) motion, (c) convective updraft component (computed as the convective mass flux divided by the ambient air density), (d) effective velocity (V_e) for HNO_3 due to gravitational settling of cloud water/ice, STDFALL.

than one layer before evaporating or sublimating, given the long potential survival distances computed by previous studies (Heymsfield and Donner, 1990; Hall and Pruppacher, 1976, who computed that ice particles could fall more than 2 km even when the sub-cloud relative humidity is below 70%). In addition, we do not allow any cloud particles to settle out of the bottom layer of the model (i.e., we set $V_t = 0$ for the surface layer). Thus, the gravitational settling process as modeled here is mass-conserving, i.e. whatever is removed from one layer is added to the layer below.

Table 3. *Summary of model simulations*

Case	V_t(ice) (cm/s)	V_t (liq) (cm/s) land	V_t (liq) (cm/s) sea	F_p (ice) HNO_3	F_p (ice) H_2O_2	Fig. HNO_3	Fig. H_2O_2
BASE	no settling	no settling		—	—	3a, 4	9a, 10
STDFALL	equation (1)	1.5	2.8	1.0	Table 2	3b, 4	9b, 10
STDVI+4VL	equation (1)	6.0	11.2	1.0	—	4	—
HIUPTAKE	equation (1)	1.5	2.8	—	1.0	—	10, 11a
SLOWICE	5.0	0	0	1.0	Table 2	6a	11b
LOWUPTAKE	5.0	0	0	limited to 10^{14} molec/cm^2	—	6b	—
STDLIQ	0	1.5	2.8	—	—	7a	11c
FASTLIQ	0	6.0	11.2	—	—	7b	11d

Each case is run individually for gravitational settling acting on either HNO_3 or H_2O_2 (with the exception of STDVI+4VL and LOWUPTAKE, which are only done for HNO_3, and HIUPTAKE, which is only done for H_2O_2).

The last two columns give the figures in which the simulation results can be found; if no entry is given, then the run was not done for that particular trace gas.

For all cases, F_p for liquid clouds is based on Henry's law.

3. Results

3.1. Nitric acid

The downward settling velocities depicted in Fig. 2 would be expected to significantly impact the HNO_3 amounts in the MATCH simulation. This is indeed the case, as can be seen in Fig. 3, which shows the July zonal mean HNO_3 distribution for the BASE run, along with the change in HNO_3 for STDFALL. There is a strong reduction in the HNO_3 amount throughout the upper troposphere, due to the downward flux from gravitational settling. Because of the large difference between the assumed ice and liquid settling velocities, there is a notable increase in HNO_3 throughout most of the lower troposphere (due to release of HNO_3 by sublimating falling particles). This "piling up" of HNO_3 below the freezing altitudes has the effect of increasing the amount of HNO_3 which is lost by wet and dry deposition (which are more efficient closer to the surface), thus

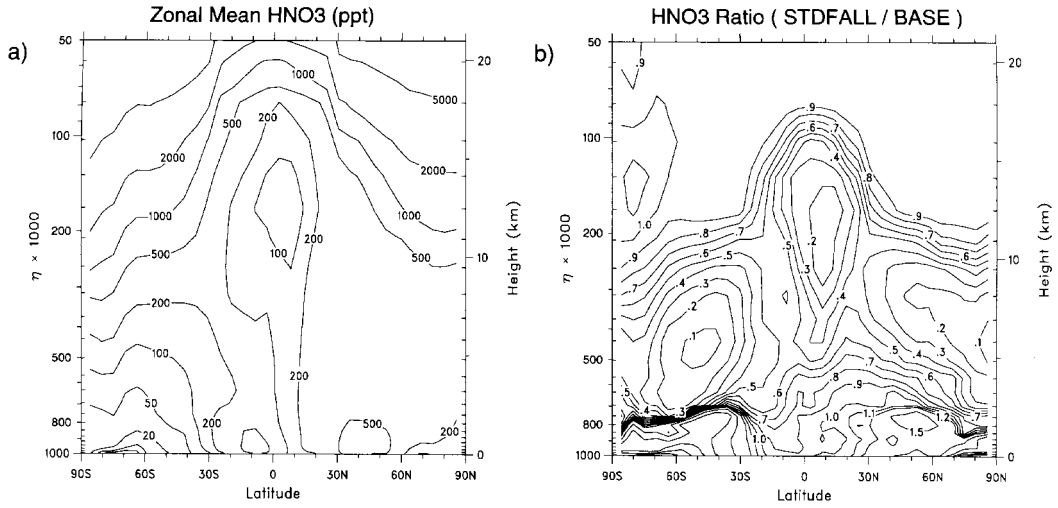

Fig. 3. The effect of gravitational settling on HNO_3. Plotted are: (a) the simulated July zonal mean distribution of HNO_3 (pptv) for the BASE run; (b) the July zonal mean ratio of HNO_3 in the STDFALL run relative to the BASE run.

reducing the integrated amount of HNO_3 computed to be in the troposphere in July from 0.53 Tg in the BASE Run to 0.39 Tg in STDFALL (recall that we model the gravitational settling process itself as being mass-conserving by not allowing HNO_3 to settle out of the bottom layer of the model, so that the decrease in total HNO_3 is only due to increased dry and wet depositional fluxes).

It was noted in the introduction that MATCH and several other GTPMs tend to substantially overestimate free tropospheric HNO_3 amounts in comparison to data from several observational campaigns. This overestimate can be seen in Fig. 4 by comparing the HNO_3 levels from the MATCH BASE run run (solid line) to the observed mean profiles (squares and triangles) for the regions depicted in Fig. 5 (the observations are from the compilation in Thakur et al., 1998). In all twelve regions for which data was available, the upper tropospheric HNO_3 mixing ratios computed in the MATCH BASE run are higher than observed. In some regions (particularly off the US west coast, over Alaska, and over Canada/Greenland — regions 3, 4, and 15, respectively), this overestimate is quite substantial. In these three regions, because of the steep gradients of increasing HNO_3 with altitude, it would appear that the stratosphere-troposphere exchange (STE) source of HNO_3 might be overestimated in these simulations, particularly since the regions are generally in the vicinity of the jet stream where STE is strongest. This particular feature of the BASE simulation needs to be borne in mind in examining the results below.

There are also a few significant differences in the lower troposphere. Near the surface of region 14, the extremely high observed HNO_3 mixing ratios (>2 ppbv) are presumably directly influenced by continental (or island) industrial emissions, whereas region 14 for the MATCH grid is entirely marine, and thus shows much less HNO_3. In regions 9 and 10, the MATCH BASE run predicts a large peak in HNO_3 around 2 km, due to outflow of biomass burning emissions from Africa. This is also present, though weaker, in the observations in region 10. In the 1993 NCEP data (used to drive these simulations), the September easterlies over southern-central Africa are strongest around 700–800 hPa (2–3 km). These winds carry biomass burning influenced air masses with high NO_x and HNO_3 concentrations into regions 9 and 10; thus, the peak in region 10 is weaker than that in region 9 due to due to loss of HNO_3 underway (mainly to wet deposition). It is possible that the overestimate of these peaks in the simulation is due to interannual variability of either the biomass burning emissions intensity or the continental outflow characteristics (the observations are for a different year, 1992, than the 1993 model meteorology), or perhaps due to the limited temporal coverage of the sampling (so that a monthly mean was not truly sampled). We will leave this particular discrepancy for future study and focus on the general overestimate of free tropospheric HNO_3 amounts seen for all regions in the BASE run.

When we include gravitational settling in the model simulation (dashed line — STDFALL), we find strongly reduced free tropospheric HNO_3 amounts. These reductions generally correspond to where clouds are most prevalent (the vertical profile of cloud fraction within each region is shown as the dotted line). This brings the simulated HNO_3 into much closer agreement with the observations in the mid and upper troposphere in nearly all the regions. In about half of the regions, however, an overestimate of HNO_3 still persists. This might indicate that the upper tropospheric settling effect has been underestimated in these regions, or that there are errors in the HNO_3 sources and sinks due to other processes.

In contrast to the reductions in the upper troposphere, the introduction of settling into the simulation results in a notable lower-tropospheric maximum ("bulge") in the HNO_3 profile in four regions (2, 3, 4, and 15). This is due to deposition of HNO_3 via sublimating hydrometeors settling into the lower free troposphere. The model cloud profiles (dotted lines) show a minimum cloud fraction coinciding with the bulge in each region, which will limit settling out of the lower troposphere; thus HNO_3 settles in from above much more quickly than it can be removed, forming the bulges. (Note that these bulges look similar to the 2 km maxima in regions 9 and 10, which were already present before settling was introduced, but come about for an entirely different reason.) Interestingly, a tenuous lower-tropospheric maximum is also present in the observations in Regions 2, 3, and 4, but it is much weaker than that computed by the model in the STDFALL

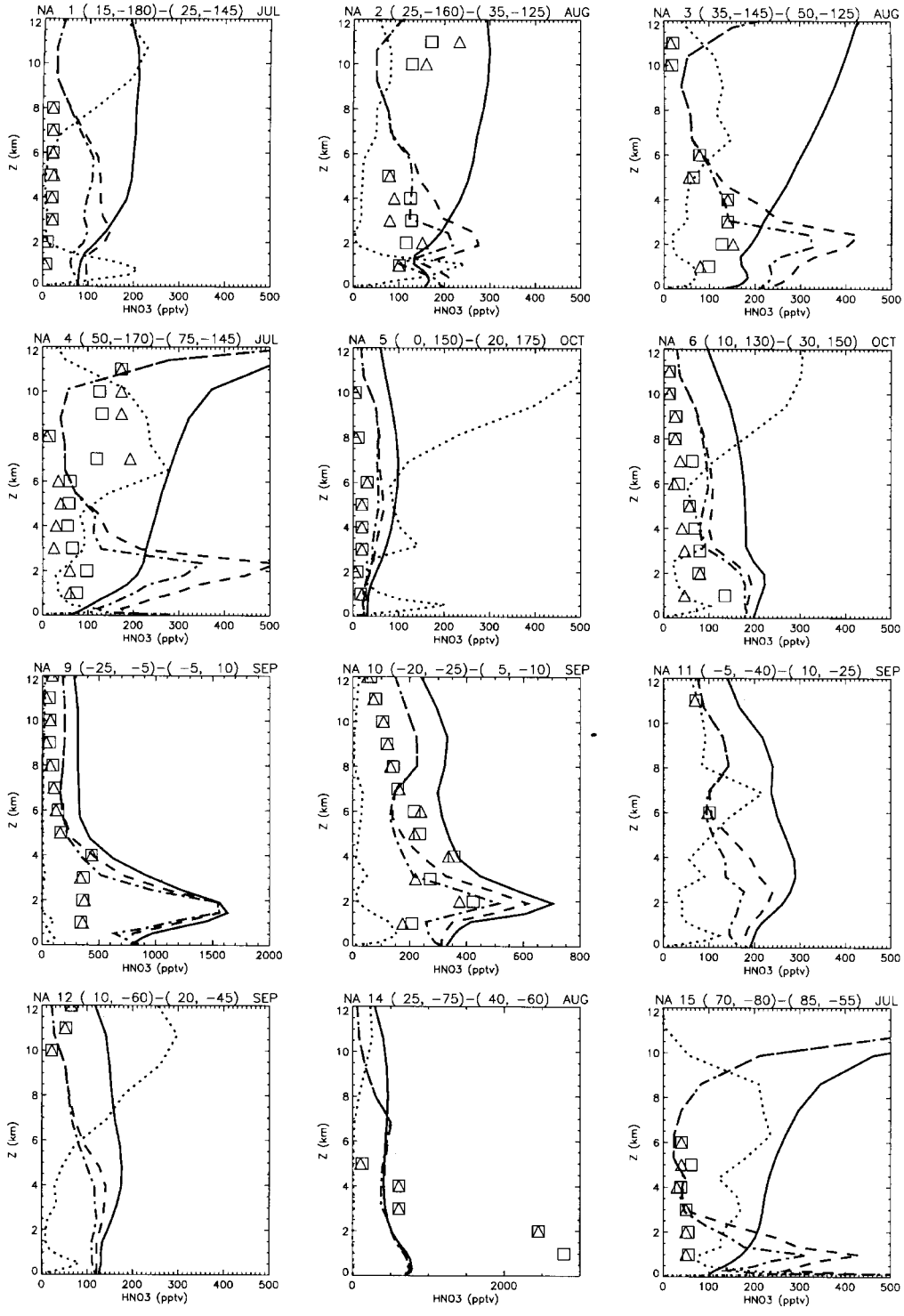
NA 1 (15,-180)-(25,-145) JUL
NA 2 (25,-160)-(35,-125) AUG
NA 3 (35,-145)-(50,-125) AUG
NA 4 (50,-170)-(75,-145) JUL
NA 5 (0, 150)-(20, 175) OCT
NA 6 (10, 130)-(30, 150) OCT
NA 9 (-25, -5)-(-5, 10) SEP
NA 10 (-20, -25)-(5, -10) SEP
NA 11 (-5, -40)-(10, -25) SEP
NA 12 (10, -60)-(20, -45) SEP
NA 14 (25, -75)-(40, -60) AUG
NA 15 (70, -80)-(85, -55) JUL
Z (km)
HNO3 (pptv)

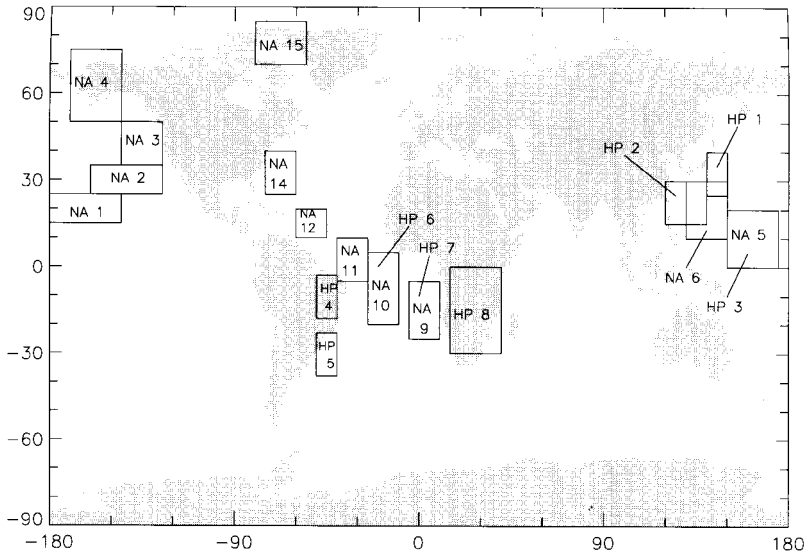

Fig. 5. The regions for which the observed mean HNO_3 and H_2O_2 profiles in Figs. 4 and 10 have been compiled. Regions labeled "NA #" are for nitric acid observations; "HP #" are for hydrogen peroxide. All regions are rectangular; the exact dimensions of the regions are listed in Figs. 4 and 10. In some instances, the sampling regions overlap; where overlapping is close but not exact, only the corresponding region for HNO_3 is depicted to avoid confusion. Note that region numbers for HNO_3 correspond to those in Thakur et al. (1998); there is no data for three regions in their compilation (regions 7, 8, and 13).

run. There are several possible reasons why the model overestimates the strength of this lower tropospheric bulge. One is that there is too little lower-tropospheric cloud in the model simulations. Assessment of this, however, is hindered by the difficulty in reliably determining the climatological mean vertical profile of cloudiness over a given location, particularly for oceanic regions (2 and 3). This leaves open other possible explanations for the overestimated bulge. It was mentioned earlier that liquid droplet settling velocities might be considerably higher than our standard values. Although the low cloud fractions will limit the effect of liquid settling out of the bulge regions, we can still test this possibility by increasing the liquid fall velocities to four times those used in STDFALL (but keeping the same ice terminal velocities as in STDFALL). The results from this simulation (STDVI+4VL) are also shown in Fig. 4 (dash-dot line). This reduces the severity of the bulges, but they remain much stronger than observed. Another possibility is that HNO_3 is being scavenged by ice particles which survive relatively long fall distances in the lower troposphere below the cloud bases; recall that we have chosen to neglect this effect by only considering settling from one (cloudy) cell into the next underlying cell. Yet another possibility is that the STE source of HNO_3 is too strong over the bulge regions, so that too much HNO_3 is being provided to the settling ice particles in the upper and mid troposphere, in turn providing too strong a source of HNO_3 to the lower troposphere. This would seem particularly plausible, since the bulge is strongest for the regions (3, 4, and 15) where it was indicated earlier that the STE source of HNO_3

Fig. 4. Regional mean observed and simulated HNO_3 profiles. The region numbers, bounding coordinates, and month are listed in each frame heading, and the regions are depicted in Fig. 5. The symbols are: squares — observed median; triangles — observed mean; solid line — BASE run; dashed line — STDFALL; dash-dot line — STDVI+4VL; dotted line — cloud fraction ($\times 1000$). Note that the x-axis scale differs for some of the frames. Note also that the meteorology used to force the model is for a different year (1993) than most of the observations (which are scattered over several years depending on the region).

appears to be too strong. A final possibility is that we may be missing some process which removes gas phase HNO_3 from the lower troposphere (predominately at higher latitudes), e.g., reactions on aerosol particles, or partitioning into the aerosol nitrate phase (D. J. Jacob, personal communication, 1997). All of these possibilities require further consideration in future studies.

On the whole, the introduction of the settling mechanism leads to a substantial improvement in the agreement between the computed and observed HNO_3 profiles, particularly in the upper troposphere, although it also leads to an overly strong lower tropospheric maximum in some regions. Further investigation of the kinds of discrepancies that are present after the gravitational settling mechanism is incorporated might not only lead to a better understanding of how to model the mechanism itself, but also help to point out other processes which are at present inadequately simulated (e.g., STE, or heterogeneous processes).

We now turn our attention to considering the sensitivity to ice and liquid cloud particle settling individually. To examine the degree of sensitivity to ice settling, we conducted a simulation (SLOWICE) in which we set V_t for ice to 5 cm/s. This is at the low-end of what is generally measured and computed for mean terminal velocities, and would thus represent the mean terminal velocity for a cloud composed only of rather small ice crystals. We also set the liquid fall velocities to zero to isolate the effect due to ice particle settling. The results of this simulation are plotted in Fig. 6a, which shows that even under the assumption of a low-end terminal velocity, the downward forcing of HNO_3 due to gravitational settling results in a marked reduction throughout most of the upper troposphere, and an increase in the lower troposphere (where settled HNO_3 is deposited). The response to even this low terminal velocity is surprisingly strong, in some regions being nearly as strong as the effect seen for STDFALL (Fig. 3). We have found (not shown) that if we increase the assumed V_t everywhere to 20 cm/s, we obtain a similar result to STDFALL throughout much of the troposphere. This is apparently due to the stochastic nature of clouds. If a cloud in a certain region remains for a long enough time that gravitational settling can completely empty the region of HNO_3, then increasing the settling velocities will not lead to any more HNO_3 depletion during the lifetime of the cloud (since it is all depleted from the cloud volume in the first place). This would imply that for our simulations, a typical cloud lifetime is of the order of 2 h, which gives enough time for a 20 cm/s settling velocity to empty the cloudy part of a 1–2 km thick layer; further increasing the settling velocities will thus be able to do little in the way of depleting more HNO_3 from the regions where clouds are prevalent.

It was indicated in the previous section that there is still some uncertainty about the uptake efficiency of HNO_3 onto ice crystals. It is possible, if HNO_3 is not incorporated into the bulk phase of ice, that the uptake is limited to 10^{14} molec/cm^2, as measured by Abbatt (1997). We assess the significance of this uncertainty here by computing a coverage-limited value for F_p, as discussed earlier. The effect of including this limitation in the simulation (LOWUPTAKE) is shown in Fig. 6b. The limitation is important in some regions, particularly the tropical mid-troposphere, where IWCs (and thus surface area densities) are computed to be generally too small to support the full amount of HNO_3 present in the cloudy parts of the grid cells. In other regions, particularly the tropical upper troposphere and the southern mid-latitudes mid- troposphere, the limitation has little impact on the reduction in HNO_3 computed to be caused by gravitational settling. Thus, though the potential limitation of the amount of HNO_3 which will be taken up by ice particles does not appear to qualitatively change the result of the significance of the settling mechanism, it appears to be important enough to a quantitative assessment that it is necessary to know whether HNO_3 is incorporated into the bulk ice phase. In addition, eq. (3) is approximate and applicable mainly for the types of clouds examined during CEPEX (detached anvils in the tropics); if HNO_3 is indeed only limited to residing on the ice particle surfaces, then better estimates of the surface area densities based on individual cloud characteristics will be needed from the microphysical parameterization in future studies.

Although thus far we have focused primarily on the effect due to the settling of ice in the upper troposphere, there is also an important effect from settling of liquid cloud droplets. We have done two additional simulations in which V_t for ice was set to zero, and either low or high fall velocities

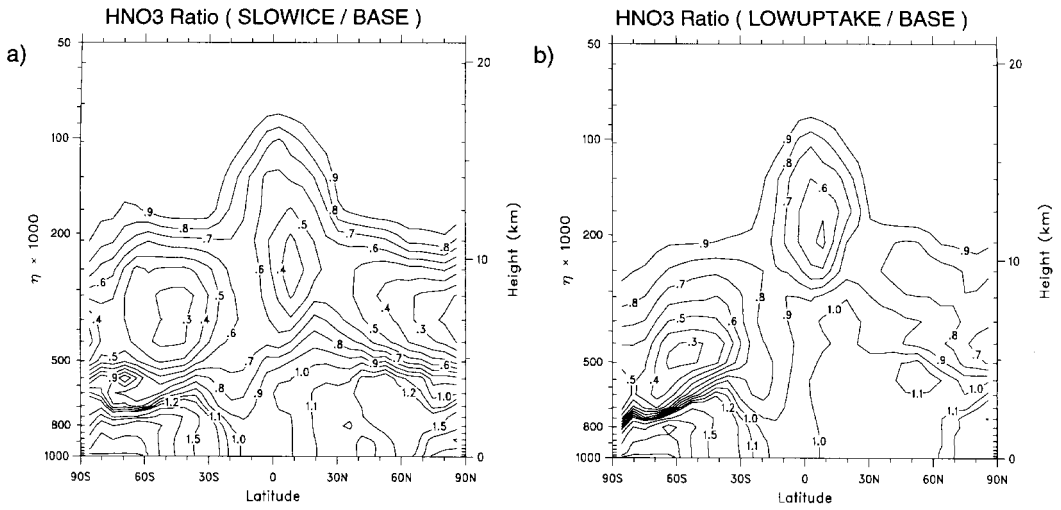

Fig. 6. The effect of ice particle settling on the HNO_3 distribution. Plotted are the July zonal mean ratios of HNO_3 (relative to the BASE run) for: (a) SLOWICE; (b) LOWUPTAKE.

for liquid water were employed (STDLIQ and FASTLIQ). The change in HNO_3 relative to the BASE run resulting for these two simulations is shown in Fig. 7. For STDLIQ, with slower fall velocities derived from the satellite-based mean droplet radii of Han et al. (1994), we compute a reduction of up to 40% in mid-tropospheric HNO_3 amounts. This effect was hidden in the earlier STDFALL simulation (Fig. 3) by the additional flux of HNO_3 into the mid troposphere due to settling of ice particles from higher altitudes. For FASTLIQ, in which we employ liquid settling velocities which are four times as high (based on the larger mean radii indicated in Heymsfield, 1993, and taking into account the possibility that HNO_3 will be predominantly taken up in larger

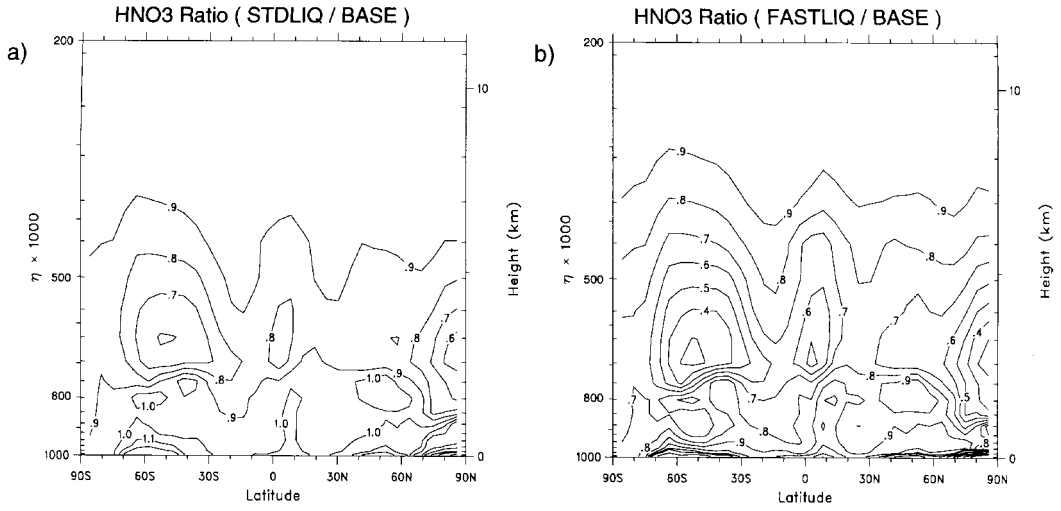

Fig. 7. The effect of liquid droplet settling on the HNO_3 distribution. Plotted are the July zonal mean ratios of HNO_3 (relative to the BASE run) for: (a) STDLIQ; (b) FASTLIQ. Note that the vertical axis is zoomed in to show only the region below about 200 hPa.

droplets), we find reductions of up to 70%, and exceeding 20% for all of the lower to mid troposphere. Thus, the gravitational settling of liquid cloud droplets could be of significance for tropospheric chemistry, and more precise effective fall velocities to apply to soluble gases in global models need to be determined.

Finally, the direct impact of gravitational settling on simulated HNO_3 amounts will also have an indirect effect on other trace gases, in particular NO_x and OH. To see how large this impact could be, we plot the change in NO_x and OH distributions for STDFALL in Fig. 8 (O_3 is not plotted; we found the change in zonal mean ozone levels to be less than 10% in our STDFALL simulation). Free tropospheric NO_x amounts are reduced in this simulation by 20–50%. The simulated NO_x levels tend to be slightly underestimated in the BASE run compared to observations (not shown); thus, the incorporation of settling degrades the comparison between computed and observed NO_x profiles. The reason for the underestimate in the BASE run is not yet known. Since the underestimate is generally most significant in the upper troposphere, it might indicate that either the simulated lightning NO_x source or the stratosphere-troposphere exchange source of NO_x are too small; this is being examined in ongoing studies.

The decrease in OH levels computed for the STDFALL run (Fig. 8b) exceeds 10% throughout much of the free troposphere. This decrease is due to two factors: (1) the decrease in NO_x (Fig. 8a) will tend to cycle less HO_2 back to OH via reaction of $NO + HO_2$, and will shift the methane oxidation cycle away from HO_x production and towards HO_x consumption; (2) HO_x is tied up in HNO_3 via the reaction $OH + NO_2$, so that the settling redistribution of HNO_3 is also a direct removal of HO_x from a layer. The first mechanism is already a well-known relationship between NO_x and OH levels (e.g., Crutzen, 1994). The potential for the second mechanism to contribute to HO_x loss on a large spatial scale can be readily estimated from the data in Figs. 2, 3. For example, in the tropical upper troposphere, the zonal mean settling velocity is about 10 cm/s, and the zonal mean HNO_3 mixing ratio (after settling is applied) is about 20 ppt, or about 10^8 molec/cm^3. This implies a downward flux of about 10^9 molec/cm^2/s. The mean (24-h) production rate of HO_x in the upper troposphere is about 10^5 molec/cm^3/s. The loss of HO_x via HNO_3 settling out of a model layer is given by the HNO_3 flux divided by the layer depth (about 10^5 cm), which yields about 10^4 molec/cm^3/s, or about 10% of the HO_x production rate. This is about the same amount as the reduction in HO_x seen in Fig. 8b, indicating that direct loss of HO_x via the HNO_3 settling loss can indeed play a role. The relative role of this versus the reduction in NO_x will vary regionally, depending on the photochemical nature of the region.

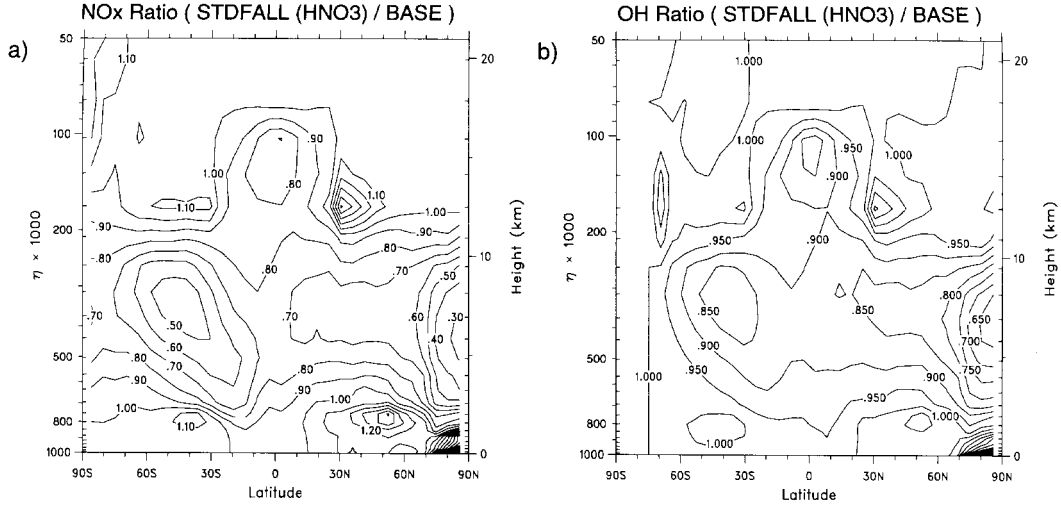

Fig. 8. The July zonal mean ratio of (a) NO_x, and (b) OH, for STDFALL (HNO_3 settling) relative to the BASE run.

3.2. *Hydrogen peroxide*

In this section, we consider the impact that gravitational settling of cloud particles can have on H_2O_2. We conduct the set of runs listed in Table 3 for H_2O_2. The July zonal mean distribution of H_2O_2 in the BASE run is depicted in Fig. 9a. The H_2O_2 mixing ratio decreases with altitude, following its primary precursor, HO_2. Since H_2O_2 has a lifetime due to photochemical and precipitation scavenging losses of one to a few days in the free troposphere, one might expect that gravitational settling at the velocities discussed earlier could lead to a significant reduction in free-tropospheric H_2O_2 amounts. When we incorporate gravitational settling into the simulation, we do indeed compute a substantial decrease in the H_2O_2 mixing ratios in the upper troposphere; this is shown in Fig. 9b for the STDFALL run. The computed zonal mean relative reduction exceeds 70% for parts of the tropical and winter high-latitudes upper troposphere.

Similar to HNO_3, observations of H_2O_2 have been obtained during several measurement campaigns. We compare our simulation results to these observed profiles in Fig. 10 (the data are the same as used in Wang et al., 1998). The BASE case values (solid lines) both underestimate and overestimate the observed H_2O_2 (squares and triangles), depending on the region. The largest differences are in the lower troposphere. Over regions 4 and 5 (Brazil), the underestimate is perhaps due to neglect of non-methane hydrocarbon chemistry in our MATCH simulations, which could provide an additional source of peroxides. In regions 6 and 7 (South Atlantic and African Coast), the peaks in H_2O_2 just below 800 hPa are due to outflow of biomass burning emissions from Africa, similar to what was previously indicated to be the cause for the lower-tropospheric HNO_3 maxima in the same regions (NA 9 and NA 10, in Fig. 5). In the upper troposphere, H_2O_2 is overestimated about as often as it is underestimated, i.e., there is no clear signal for an overestimate in our BASE run like there was for HNO_3. When we include gravitational settling in the STDFALL run (dashed lines), we find little difference in the comparison of the H_2O_2 profiles. This is because the main influence of settling in the STDFALL run is above 200 hPa (due to the temperature dependence in Table 2), while the ceiling of the measurements was just below the 200 hPa level. For the HIUPTAKE run, we compute a larger influence in the mid-troposphere, and a greater tendency for H_2O_2 amounts to increase in the lower troposphere. These changes, however, make no clear difference in the degree of agreement or disagreement with the observations. Thus, due primarily to the limited altitude

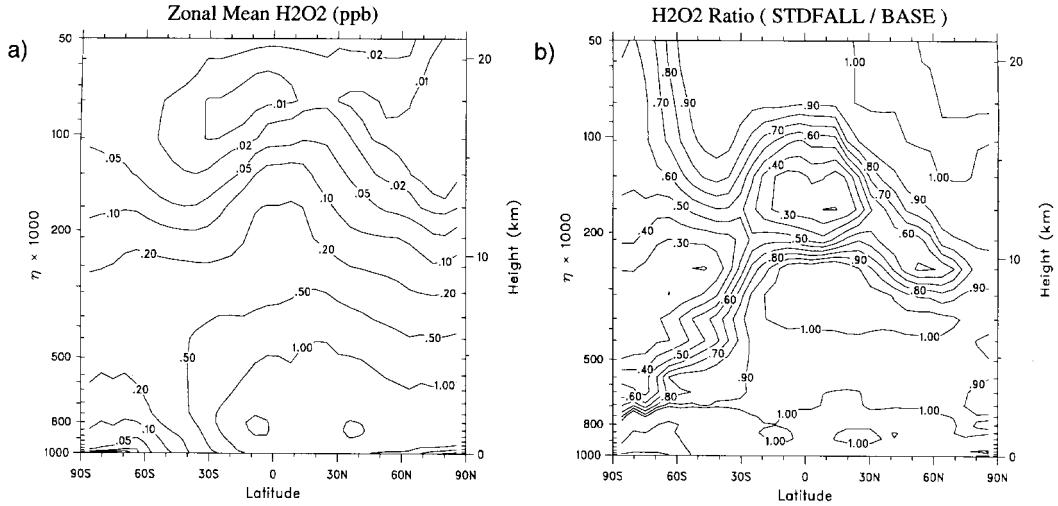

Fig. 9. The effect of gravitational settling on H_2O_2. Plotted are: (a) the simulated July zonal mean distribution of H_2O_2 (ppbv) for the BASE run; (b) the July zonal mean ratio of H_2O_2 in STDFALL relative to the BASE run.

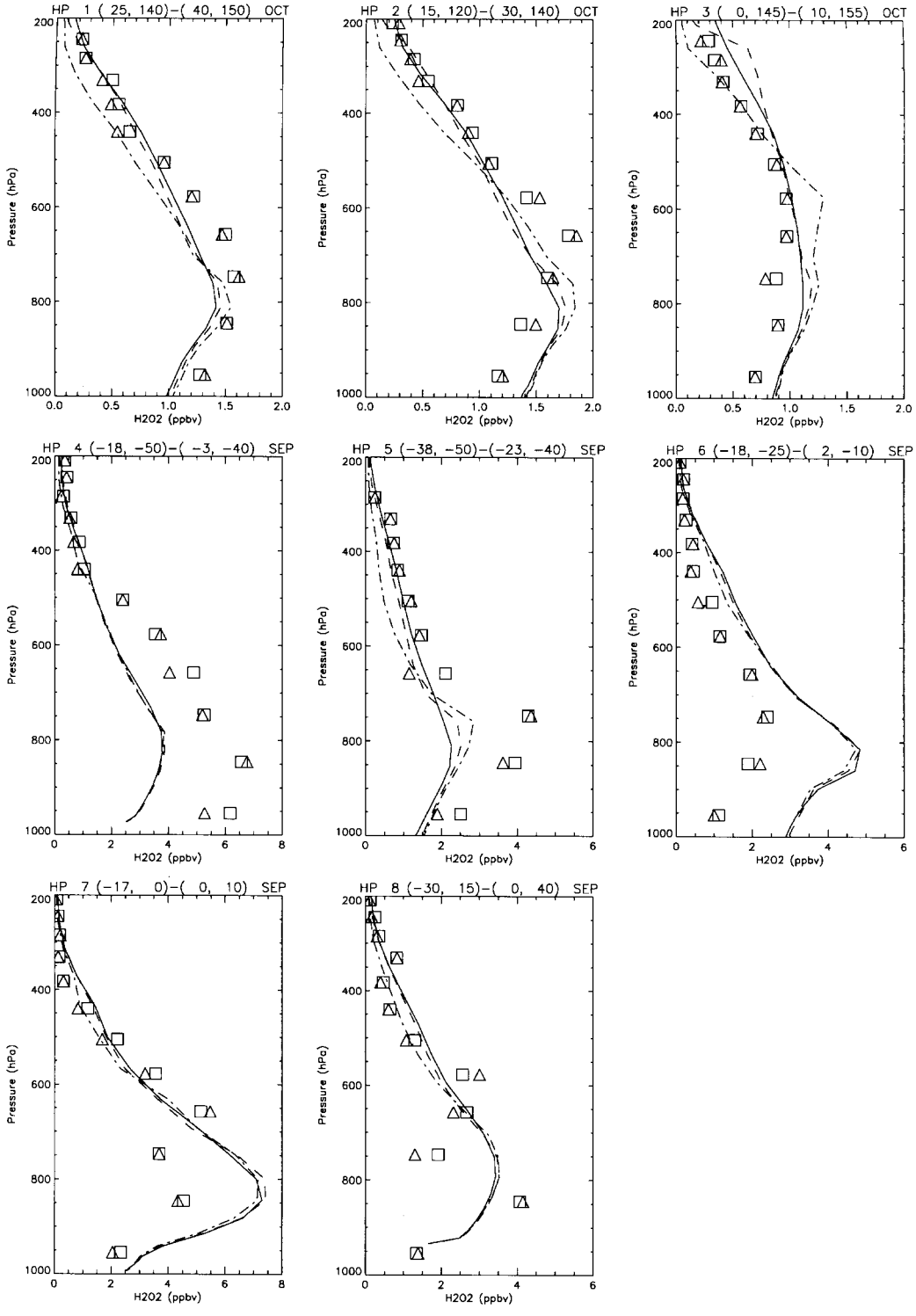
HP 1 (25, 140)-(40, 150) OCT
HP 2 (15, 120)-(30, 140) OCT
HP 3 (0, 145)-(10, 155) OCT
HP 4 (-18, -50)-(-3, -40) SEP
HP 5 (-38, -50)-(-23, -40) SEP
HP 6 (-18, -25)-(2, -10) SEP
HP 7 (-17, 0)-(0, 10) SEP
HP 8 (-30, 15)-(0, 40) SEP
Pressure (hPa)
H2O2 (ppbv)

coverage of these measurements, the comparison to observations provides little support for or evidence against the effect of gravitational settling on H_2O_2. Future measurements of H_2O_2 in the upper tropical troposphere might provide greater insight along these lines.

The amount of redistribution of H_2O_2 by gravitational settling is quite sensitive to the assumed uptake partitioning coefficients listed in Table 2. This can be seen in the results for the HIUPTAKE run (Fig. 11a), which show a reduction in H_2O_2 extending considerably further down into the mid-troposphere than for the STDFALL run. The difference is due to the temperature dependence of the uptake partitioning coefficient; less H_2O_2 is expected to be partitioned into the ice phase at higher temperatures (lower altitudes) in the STDFALL run (note that the partitioning also depends on the ice water content, which generally increases with temperature, but the partitioning coefficient changes more rapidly with temperature than the ice water content). Although the partitioning coefficients used here do not qualitatively change our result of a significant depletion of upper tropospheric H_2O_2, there is a strong quantitative dependence on the uptake temperature dependence — especially in the range where we extrapolate the curve to temperatures below the lowest measurements ($-45^{\circ}C$) — which should encourage further laboratory studies of this process. The strong potential sensitivity of H_2O_2 to gravitational settling of ice crystals is also seen in Fig. 11b, which shows the ratio of the H_2O_2 distribution for the SLOWICE case relative to the BASE run. Even for these limited conditions, H_2O_2 is reduced by more than 30% in the upper tropical troposphere. When we instead assume a 100% uptake efficiency on ice, but keep the 5 cm/s ice settling velocity, we compute a reduction of 30–50% throughout most of the tropical and northern hemisphere upper troposphere (not shown), again indicating the importance of the temperature dependence of the partitioning coefficients in Table 2.

Since H_2O_2 is less soluble than HNO_3, it should be expected that the settling of liquid droplets alone would have a less significant impact on H_2O_2. This is seen in Fig. 11(c,d), which shows the results for the STDLIQ and FASTLIQ cases. For STDLIQ, the reduction only exceeds 10% for the polar regions, where H_2O_2 is particularly susceptible to the forcing from gravitational settling due to the slow photochemical production there. When we increase the liquid fall velocities to four times as fast (FASTLIQ), we compute up to a 20% reduction in the tropical mid troposphere (and an ostensibly larger change in the polar regions).

Finally, because H_2O_2 plays a role in the HO_x budget, one might anticipate that the changes in H_2O_2 due to gravitational settling computed here would result in reductions in global OH amounts. In Fig. 12, a small change in OH is indeed seen: the computed OH levels in the upper tropical troposphere in the STDFALL run are reduced by about 10%, and in the winter mid-latitudes by about 20%.

4. Discussion and conclusions

This study has examined the impact of the gravitational settling of smaller ("non-precipitate") hydrometeors on global nitric acid and hydrogen peroxide distributions. It was found that this can lead to a substantial reduction in simulated HNO_3 and H_2O_2 levels in the free troposphere, as well as an increase in their amounts near the surface in some regions. The computed significance of gravitational settling is rather robust for both HNO_3 and H_2O_2: even when we use a low-end ice particle settling velocity of 5 cm/s (and assume that HNO_3 is not incorporated into the ice bulk phase), we calculate maximum zonal mean reductions of greater than 50% for HNO_3 and 40% for

Fig. 10. Regional mean observed and simulated H_2O_2 profiles. The region numbers, bounding coordinates, and months are listed in each frame heading, and the regions are depicted in Fig. 5. The symbols are: squares — observed median; triangles — observed mean; solid line — BASE run; dashed line — STDFALL; dash-dot line — HIUPTAKE. Note that the *x*-axis scale is not the same for all frames. Note also that the meteorology used to force the model is for a different year (1993) than most of the observations (which are scattered over several years depending on the region).

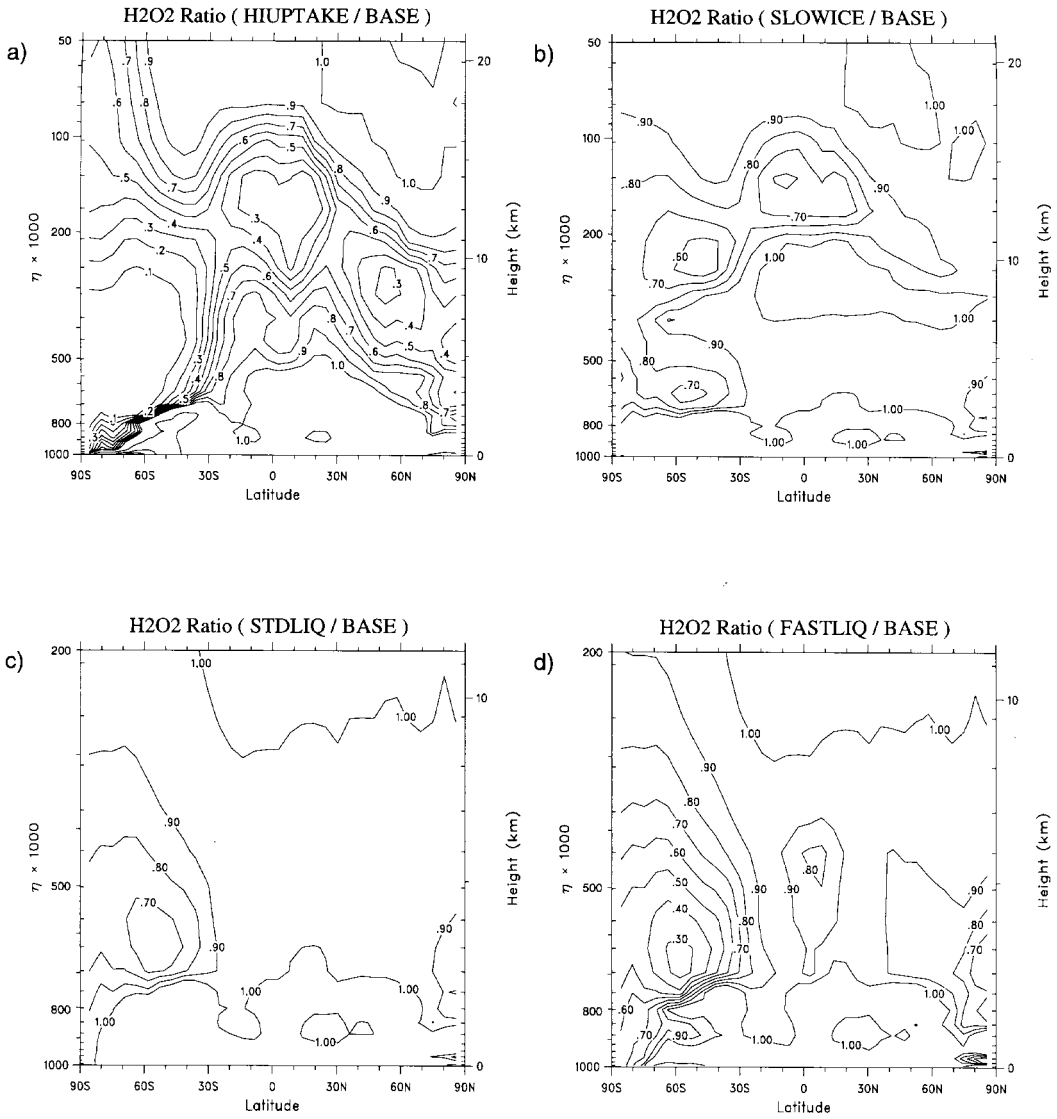

Fig. 11. Sensitivity simulations of the effects of ice particle and liquid droplet settling on the H_2O_2 distribution. Plotted are the July zonal mean ratios of H_2O_2 (relative to the BASE run) for: (a) HIUPTAKE, (b) SLOWICE, (c) STDLIQ, (d) FASTLIQ. For the latter two panels, the vertical axis is zoomed in to show only the region below about 200 hPa.

H_2O_2 in the tropical upper troposphere. In addition, incorporation of the settling mechanism can also lead to indirect reductions in the computed NO_x and OH amounts in the free troposphere.

There are several uncertainties with regards to this mechanism which need to be considered in more detail in future studies. The uptake of HNO_3 and H_2O_2 onto and into ice was discussed in this work, and shown to still be a highly uncertain parameter in the settling mechanism. Further laboratory studies are needed to address several issues, such as: the degree to which these species

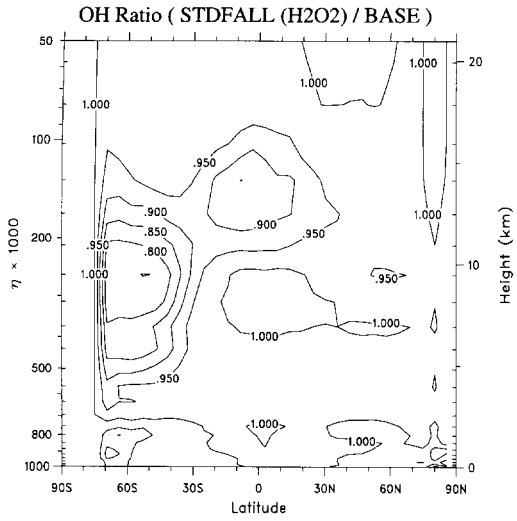

Fig. 12. The July zonal mean ratio of OH for STDFALL (H_2O_2 settling) relative to the BASE run.

are incorporated into the ice bulk phase; the influence of particle growth (via water vapor deposition) on the uptake efficiency; the degree of trapping of trace gases when supercooled droplets freeze; the exact form of any temperature dependencies, especially at very low T, where our assumptions for H_2O_2 (Table 2) are extrapolated from the data (and thus are relatively uncertain); and the extent to which heterogeneous reactions (e.g., $H_2O_2 + S(IV)$) might irreversibly convert the trace gases to other forms before gravitational settling can take effect. In addition, further field studies along the lines of that performed by Weinheimer et al. (1998) will help give a better understanding of the uptake of trace gases under various meteorological conditions.

Another major uncertainty in our simulations is the quality and representativeness of the microphysical and meteorological parameters used in the settling algorithm. In particular, the ice terminal velocity values employed here are based on in situ observations in only a few sets of clouds. Furthermore, the liquid settling velocities are quite different depending whether they are derived from satellite-based or in situ-based mean droplet radii. These velocities will therefore not necessarily capture the regional variability in cloud characteristics. However, we expect them to be sufficiently representative of the "average" cloud on a global basis provide a decent first estimate of the global impact of gravitational settling. On a similar note, there is a significant potential for our modeled cloud fractions to deviate from the actual climatological distribution, since our cloud fractions are based on a relatively simple parameterization (determined mainly as a function of the large scale relative humidity, from Slingo, 1987). In particular, our modeled distributions will differ in terms of the vertical extent of clouds (which, recall, are assumed to extend from layer base to top when present, which is often thicker than actual cloud layers). Again, however, based on comparisons of our zonal mean cloud distribution with cloud atlas data (Warren et al., 1986; Lelieveld et al., 1989), we feel confident that our model cloud distribution is sufficiently representative of the actual global climatological distribution to give a reasonable first estimate of the global impact of gravitational settling. Improvements in our understanding of both microphysical and large-scale meteorological parameters on a global scale will clearly be valuable for future global studies of gravitational settling.

Apart from cloud-related parameters, another sub-gridscale process which is difficult to handle in global models is large scale (non-convective) vertical motion. It was indicated in the introduction that at present global models can only make fairly crude approximations to the small-scale "patchwork" motions that will occur within a grid cell. On a cloud scale, it is possible for ambient upward motion to be faster than the mean settling velocity of the cloud particles, resulting in a net upward motion of the cloud and trace gases contained within its particles. Our simulations will generally not capture this feature of the settling mechanism, since our large-scale vertical velocities averaged over the dimensions of a grid cell will usually be much slower than the settling velocities within an individual cloud. However, they will capture the pertinent process which settling represents: a *separation* of soluble and non-soluble trace gases. The key point is that regardless of the small scale details, soluble trace gases will have a vertical velocity which is more negative (downwards) than non-soluble trace gases, due to the sedimentation of the media in which the soluble trace gases reside (cloud droplets and particles). Determining how these sub-gridscale motions affect our quant-

itative estimate of the global impact of gravitational settling will require future studies with a model that is capable of resolving such motions.

Another uncertainty in the impact of gravitational settling which we did not consider is that settling will directly affect the cloud water/ice distributions themselves, in turn affecting the global water vapor distribution. This will in turn have an indirect impact on global photochemistry, and possibly on the settling mechanism itself. However, incorporation of settling into our water vapor and microphysics simulations in a consistent fashion is not straightforward, because it requires altering several parameters (thresholds and conversion rates) within the microphysics module in order to still obtain cloud water/ice contents that agree well with in situ observations; thus we have not addressed this particular issue in this first study.

A final uncertainty to consider with regards to understanding the relative role of gravitational settling in determining HNO_3 and H_2O_2 distributions is that the individual roles of other important processes are in many instances still poorly known, or left out entirely. Among these processes are: the amount of loss of soluble trace gases to wet deposition (i.e., scavenging by large precipitate particles, not including gravitational settling itself); the sources of trace gases to the upper troposphere via convective transport (including possible transport of soluble trace gases within cloud particles that are small enough to be carried upwards in the core updrafts); heterogeneous reaction losses and partitioning into the aerosol phase; photochemical formation rates, in particular due to uncertainties in HO_x and NO_x concentrations, and due to the influence of non-methane hydrocarbons; and mixing by sub-gridscale vertical transport (both in cloudy and cloud-free regions).

It is worth pointing out that several assumptions which were made regarding the treatment of gravitational settling in our STDFALL case might make our results a lower limit to the global effect. For instance, we did not allow the settling of hydrometeors to redistribute trace gases more than one layer at a time, although there is evidence that ice particles are able to fall much farther than the thickness of a single model layer before sublimating (Heymsfield and Donner, 1990; Hall and Pruppacher, 1976). We also treated the settling mechanism as mass-conserving by disallowing any additional loss to the surface by settling cloud (or fog) particles in the model surface layer (only the indirect additional loss at the surface due to enhanced dry and wet deposition fluxes was allowed). Furthermore, we neglected the effect that would come from the additional scavenging of HNO_3 or H_2O_2 by settling hydrometeors below the cloud base (for instance, Weinheimer et al., 1998, computed that only about 1% of a monolayer of the ice crystals they observed would be covered by HNO_3, leaving plenty of opportunity for additional scavenging below cloud base). Finally, the settling velocities we have assumed for liquid droplets in STDFALL may be significantly underestimated due to the use of satellite-based mean droplet radii and the assumption of equal partitioning of HNO_3 among large and small droplets.

Besides HNO_3 and H_2O_2, there are other soluble trace gases which might be affected by gravitational settling. For instance, SO_2 might also be subject to settling effects, since Valdez et al. (1989) showed it is taken up on growing ice "at amounts comparable to SO_2/S(IV) aqueous equilibrium." In addition, S(IV) reacts with H_2O_2 on ice (Conklin et al., 1993b), which could lead to enhanced scavenging on cloud ice particles and conversion to sulfate, which would in turn be subject to redistribution via gravitational settling. Furthermore, aerosols contained in the falling cloud particles and droplets will also be affected by gravitational settling; the impact of this remains to be assessed.

Gravitational settling might also contribute to the partitioning of nitrate between gas and aerosol phases. Once HNO_3 is taken up into ice crystals and liquid droplets, it may persistently remain in the particles as they sublimate or evaporate. If the particles only partially or negligibly degas once highly concentrated aerosol particles are formed, then this will result in an enhancement in the nitrate content of the aerosols. In this study, we have not treated aerosol nitrate explicitly, and assumed that all HNO_3 is released to the gas phase once cloud droplets evaporate. The error caused by this assumption will need to be considered in future studies.

We have computed a sufficiently large direct effect on the distributions of HNO_3 and H_2O_2 to argue that gravitational settling should be generally included in global tropospheric chemistry

models. However, the parameters required to incorporate the settling mechanism in the manner done here may not be available in some models. For models in which cloud water/ice contents are not computed, we recommend employing an empirical relationship of cloud water/ice versus temperature (for examples, see Heymsfield, 1977, Stephens et al., 1990, Gultepe and Isaac, 1997, or the data in McFarquhar and Heymsfield, 1997). We have tested the settling mechanism in our model using some of these relationships, and have found an effect which is surprisingly similar in the zonal mean to the impact computed based on the ice water contents taken from the model's microphysical parameterization (Rasch and Kristjansson, 1998). However, there can be strong regional differences due to the large scatter in IWC among clouds (more than 3 orders of magnitude at any given temperature), and it is best where possible to employ model-generated IWCs, which will give more consistent regional responses to gravitational settling.

Several of the uncertainties considered in this section could be addressed in studies with a cloud-resolving model coupled with tropospheric photochemistry computations. The results here show a sufficient potential for an effect on the global scale to encourage such studies. These will hopefully lead to both a more explicit understanding of the microphysical details involved in gravitational settling, and to more accurate parameterizations of the sub-gridscale effects on trace gases for use in global models.

5. Acknowledgements

We would like to express our appreciation to Phil Rasch for helpful discussions throughout this work, and for providing a prototype version of his advection scheme for use here. We thank Greg McFarquhar and Andy Heymsfield for several valuable insights, as well as for providing the empirical parameterization for the terminal velocity versus ice water content based on their CEPEX data. We acknowledge A. Thakur for the HNO_3 observations compilation, and Yuhang Wang for sharing the H_2O_2 compilation used in his modeling comparisons. We appreciate constructive comments given by Frank Dentener, Uta Biermann, John Crowley, Jon Abbatt, Mark Zondlo, Natalie Mahowald, Mary Barth, Sven Metzger, Sabine Wurzler, and other colleagues. Finally, we are grateful for the thorough and thoughtful reviews given by Andy Heymsfield, Daniel Jacob, and an anonymous referee, which helped us to substantially improve this manuscript. This research was supported by the EC project SINDICATE. We would like to dedicate this paper to the memory of John Bradshaw, a pioneer in the field of measuring and understanding reactive nitrogen in the troposphere.

REFERENCES

Abbatt, J. P. D. 1997. Interaction of HNO_3 with water-ice surfaces at temperatures of the free troposphere. *Geophys. Res. Lett.* **24**, 1479–1482.

Arakawa, A. and Schubert, W. H. 1974. Interaction of a cumulus cloud ensemble with the large-scale environment. Part 1. *J. Atmos. Sci.* **32**, 674–701.

Conklin, M. H. A., Sigg, A., Neftel, A. and Bales, R. 1993a. Atmosphere-snow transfer function for H_2O_2: Microphysical considerations. *J. Geophys. Res.* **98**, 18 367–18 376.

Conklin, M. H., Sommerfeld, R. A., Laird, S. K. and Villinski, J. E. 1993b. Sulfur dioxide reactions on ice surfaces: Implications for dry deposition to snow. *Atmos. Environ* **27A**, 159–166.

Crutzen, P. J. 1994. *Global tropospheric chemistry, in low-temperature chemistry of the atmosphere*, ed. G. Moortgat et al., p. 465–498. Springer-Verlag, Berlin.

Crutzen, P. J. and Gidel, L. T. 1983. A two-dimensional photochemical model of the atmosphere 2: The tropospheric budgets of the anthropogenic chlorocarbons CO, CH_4, CH_3Cl, and the effects of various NO_x sources on tropospheric ozone. *J. Geophys. Res.* **8**8, 6641–6661.

Fahey, D. W., Kelly, K. K., Kawa, S. R., Tuck, A. F., Loewenstein, M., Chan, K. R. and Heidt, L. E. 1990. Observations of denitrification and dehydration in the winter polar stratospheres. *Nature* **3**44, 321–324.

Gultepe, I. and Isaac, G. A. 1997. Liquid water content and temperature relationship from aircraft observations and its applicability to GCMs. *J. Clim.* **10**, 446–452.

Hall, W. D. and Pruppacher, H. R. 1976. The survival of ice particles falling from cirrus clouds in subsaturated air. *J. Atmos. Sci.* **3**3, 1995–2006.

Han, Q., Rossow, W. B. and Lacis, A. A. 1994. Near-global survey of effective droplet radii in liquid water clouds using ISCCP data. *J. Clim.* **7**, 465–497.

Heymsfield, A. J. 1972. Ice crystal terminal velocities. *J. Atmos. Sci.* **29**, 1348–1357.

Heymsfield, A. J. 1977. Precipitation development in stratiform ice clouds: A microphysical and dynamical study. *J. Atmos. Sci.* **34**, 367–381.

Heymsfield, A. J. 1993. Microphysical structures of stratiform and cirrus clouds. In: *Aerosol-cloud-climate interactions* (ed. P. V. Hobbs), Academic Press, San Diego, pp. 97–121.

Heymsfield, A. J., and Donner, L. J. 1990. A scheme for parameterizing ice-cloud water content in general circulation models. *J. Atmos. Sci.* **47**, 1865–1877.

Heymsfield, A. J. and Kajikawa, M. 1987. An improved approach to calculating terminal velocities of plate-like crystals and graupel. *J. Atmos. Sci.* **44**, 1088–1099.

Heymsfield, A. J. and McFarquhar, G. M. 1996. High albedos of cirrus in the tropical pacific warm pool: Microphysical interpretations from CEPEX and from Kwajalein, Marshall Islands. *J. Atmos. Sci.* **53**, 2424–2451.

Jensen, E. J., Toon, O. B., Tabazadeh, A., Sachse, G. W., Anderson, B., Chan, K. R., Baumgardner, D., Twohy, C. H. and Gandrud, B., Heymsfield, A. J., Hallett, J., and Gary, B. 1998. Ice nucleation processes in upper tropospheric wave-clouds observed during SUCCESS. *Geophys. Res. Lett.*, in press.

Kalnay, E. et al. 1996. The NCEP/NCAR 40-year reanalysis project. *Bull. Am. Met. Soc.* **77**, 437–471.

Lawrence, M. G. 1996. *Photochemistry in the tropical pacific troposphere. Studies with a global 3D chemistry-meteorology model.* Doctoral Dissertation. Georgia Institute of Technology, 520 pp.

Lelieveld J, Crutzen, P. J. and Rodhe, H. 1989. *Zonal average cloud characteristic for global atmospheric chemistry modelling*. Glomac-report UDC 551.510.4 m CM-74, International Meteorological Institute Stockholm.

Lind, J. A. and Kok, G. L. 1986. Henry's law determinations for aqueous solutions of hydrogen peroxide, methylhydroperoxide, and peroxyacetic acid. *J. Geophys. Res.* **91**, 7889–7895.

Mahowald, N. M. 1996. *Development of a 3-dimensional chemical transport model based on observed winds and use in inverse modeling of the sources of CCl_3F, doctoral dissertation.* Massachussetts Institute of Technology, 199 pp.

Mahowald, N. M., Rasch, P. J., Eaton, B. E., Whittlestone, B. and Prinn, R. G. 1997a. Transport of ^{222}Radon to the remote troposphere using MATCH and assimilated winds from ECMWF and NCEP/NCAR. *J. Geophys. Res.* **102**, 28 139–28 152.

Mahowald, N. M., Prinn, R. G. and Rasch, P. J. 1997b. Deducing CCl_3F emissions using an inverse method and chemical transport models with assimilated winds. *J. Geophys. Res.* **102**, 28 153–28 168.

Mazin, I. P. 1995. Cloud water content in continental clouds of middle latitudes. *Atmos. Res.* **35**, 283–297.

McFarquhar, G. M. and Heymsfield, A. J. 1996. Microphysical characteristics of three anvils sampled during the Central Equatorial Pacific Experiment. *J. Atmos. Sci.* **53**, 2401–2423.

McFarquhar, G. M. and Heymsfield, A. J. 1997. Parameterization of tropical cirrus ice crystal size distributions and implications for radiative transfer: Results from CEPEX. *J. Atmos. Sci.* **54**, 2187–2200.

Mitchell, J. F. B., Senior, C. A. and Ingram, W. J. 1989. CO_2 and climate: a missing feedback? *Nature.* **341**, 132–134.

Pan, H.-L., and Wu, W.-S. 1995. *Implementing a mass flux convection parameterization package for the NMC medium-range forecast model.* NMC Office Note, no. 409, 40 pp.

Pruppacher, H. R., and Klett, J. D. 1997. *Microphysics of clouds and precipitation.* Kluwer, Dordrecht, The Netherlands, 954 pp.

Rasch, P. J. and Kristjansson, J. E. 1998. A comparison of the CCM3 model climate using diagnosed and predicted condensate parameterizations. *J. Climate*, in press.

Rasch, P. J., Mahowald, N. M. and Eaton, B. E. 1997. Representations of transport, convection, and the hydrologic cycle in chemical transport models: Implications for the modeling of short lived and soluble species. *J. Geophys. Res.* **102**, 28 127–28 138.

Roeckner, E., Arpe, K., Bengtsson, L., Cristoph, M., Claussen, M., Duermenil, L., Esch, M., Giorgetta, M., Schlese, U. and Schulzweida, U. 1996. *The atmospheric general circulation model ECHAM-4: Model description and simulation of present-day climate.* Max-Planck-Institute for Meteorology, Report no. 218, Hamburg, 90 pp.

Slingo, J. M. 1987. The development and verification of a cloud prediction scheme for the ECMWF model. *Q. J. R. Meteorol. Soc.* **113**, 899–927.

Stephens, G. L., Tsay, S.-C., Stackhouse, P. W. Jr. and Flatau, P. J. 1990. The relevance of the microphysical and radiative properties of cirrus clouds to climate and climate feedback. *J. Atmos. Sci.* **47**, 1742–1760.

Sundqvist, H. 1978. A parameterization scheme for non-convective condensation including prediction of cloud water content. *Q. J. R. Meterol. Soc.* **104**, 677–690.

Sundqvist, H. 1993. Inclusion of ice phase of hydrometeors in cloud parameterization for mesoscale and large scale models. *Beitr. Phys. Atmosph.* **66**, 137–147.

Sundqvist, H., Berge, E. and Kristjansson, J. E., 1989. Condensation and cloud parameterization studies with a mesoscale numerical weather prediction model. *Mon. Weather Rev.* **117**, 1641–1657.

Thakur, A. N., Singh, H. B., Mariani, P., Chen, Y., Wang, Y., Jacob, D. J., Brasseur, G., Mueller, J.-F. and Lawrence, M. 1998. Distribution of reactive nitrogen species in the remote free troposphere: Data and model comparisons. *Atmos. Env.*, in press.

Valdez, M. P., Dawson, G. A., and Bales, R. C. 1989. Sulfur dioxide incorporation into ice depositing from the vapor. *J. Geophys. Res.* **94**, 1095–1103.

Wang, Y., Logan, J. A. and Jacob, D. J. 1998. Global

simulation of tropospheric O_3-NO_x-hydrocarbon chemistry, 2. Model evaluation and global ozone budget. *J. Geophys. Res*., in press.

Warren, S. G., Hahn, C. J., London, J., Chervin, R. M., and Jenne, R. 1986. Global distribution of total cloud cover and cloud type amounts over land, NCAR Technical Note TN-273 + STR, Boulder.

Weinheimer, A. J., Campos, T. L., Walega, J. G., Grahek, F. E., Ridley, B. A., Baumgardner, D., Twohy, C. H., and Gandrud, B. 1998. Uptake of NO_y on wave-cloud ice particles. *Geophys. Res. Lett*., in press.

Zondlo, M. A., Barone, S. B. and Tolbert, M. A. 1997. Uptake of HNO_3 on ice under upper tropospheric conditions, *Geophys. Res. Lett*. **24**, 1391–1394.